

# Revisiting Universal Extra-Dimension Model with Gravity Mediated Decays

---

Kirtiman Ghosh,<sup>a</sup> Katri Huitu,<sup>b</sup> Rameswar Sahu<sup>c</sup>

<sup>a,c</sup>*Institute of Physics, Bhubaneswar, Sachivalaya Marg, Sainik School Post, Bhubaneswar 751005, India*

<sup>a,c</sup>*Homi Bhabha National Institute, Training School Complex, Anushakti Nagar, Mumbai 400094, India*

<sup>b</sup>*Department of Physics, and Helsinki Institute of Physics, University of Helsinki, Finland 00014*

*E-mail:* [kirti.gh@gmail.com](mailto:kirti.gh@gmail.com), [katri.huitu@helsinki.fi](mailto:katri.huitu@helsinki.fi),  
[rameswar.s@iopb.res.in](mailto:rameswar.s@iopb.res.in)

**ABSTRACT:** We explore the collider phenomenology of the fat-brane realization of the Minimal Universal Extra Dimension (mUED) model, where Standard Model (SM) fields propagate in a small extra dimension while gravity accesses additional large extra dimensions. This configuration allows for gravity-mediated decay (GMD) of Kaluza-Klein (KK) particles, resulting in unique final states with hard photons, jets, massive SM bosons, and large missing transverse energy due to invisible KK gravitons. We derive updated constraints on the model's parameter space by recasting ATLAS mono-photon, di-photon, and multi-jet search results using 139 inverse femtobarn of integrated luminosity data. Recognizing that current LHC search strategies are tailored for supersymmetric scenarios and may not fully capture the distinct signatures, we propose optimized strategies using machine learning algorithms to tag boosted SM bosons and enhance signal discrimination against SM backgrounds. These methods improve sensitivity to fat-brane mUED signatures and offer promising prospects for probing this model in future LHC runs.

---

## Contents

<b>1</b>	<b>Introduction</b>	<b>1</b>
<b>2</b>	<b>The fat brane realization of mUED scenario</b>	<b>4</b>
2.1	Matter-Gravity Interaction	5
<b>3</b>	<b>Collider Phenomenology</b>	<b>7</b>
3.1	KK-Number Conserving (KKNC) Decays	7
3.2	Gravity Mediated Decays (GMD)	8
3.3	Collider Signatures	8
3.4	Bounds from the existing LHC searches	12
3.4.1	ATLAS mono-photon plus missing transverse energy search [1]	13
3.4.2	ATLAS multi-jet plus missing transverse energy search [2]	15
3.4.3	ATLAS di-Photon plus missing transverse energy search [3]	16
3.4.4	Event Simulation	17
3.4.5	Results	18
3.5	Optimized search strategies for the Future LHC Runs	20
3.5.1	Event Generation and Object Reconstruction	21
3.5.2	Event Selection	23
3.5.3	Results	26
<b>4</b>	<b>Summary and Outlook</b>	<b>30</b>
<b>A</b>	<b>Appendix</b>	<b>33</b>
A.1	GMD widths of level-1 KK particles	33
A.2	Cut-flow chat for SRM and SRH signal regions	33
A.3	BDT classifier	33
A.4	Variables constructed for the different signal regions	37

---

## 1 Introduction

Notwithstanding the remarkable success of the Standard Model (SM), it continues to suffer from several cavities, particularly its inability to explain observational facts like the existence of Dark Matter (DM), non-zero neutrino masses/mixings, etc., on the one hand, and theoretical issues like the stability of the Higgs boson mass, the related naturalness/hierarchy problems, etc. on the other. These issues have led to a plethora of new dynamics beyond the SM (BSM). Theories with one or more extra space-like dimension(s) accessible to all or a few SM fields are of interest for various reasons. For example, the

ADD <sup>1</sup> [4–6] (seemingly) and RS <sup>2</sup> [7, 8] models provide solutions to the long-standing naturalness/hierarchy problem by postulating the existence of compactified extra-dimension(s) accessible only to gravity with the SM fields being confined to a 3-brane embedded in the extra-dimensional bulk. In the case of ADD model [4–6], for instance, gravity is allowed to propagate into ' $N$ ' number of large, flat, and compactified extra dimensions. The four-dimensional Planck mass is then diluted by the volume of the extra-dimensional space  $V_N \sim r^N$ , where  $N$  and  $r$  are the number and size of large extra dimensions, resulting in higher dimensional Planck mass around a few tens of TeV and hence offering a solution to naturalness/hierarchy problem. The introduction of warped metric in RS model [7, 8] provides an alternative solution to the same problem. On the other hand, there is a class of models wherein some or all SM fields can access the extended space-time manifold [9], whether fully or partially. Such extra-dimensional scenarios could address a plethora of issues, including some exciting ones like the existence of DM [10–12], an explanation for the number of fermion generations [13], the long lifetime of the proton [14], etc. As a result, over decades, extra-dimensional models remain some of the most extensively studied BSM scenarios. And search for the extra-dimension(s) is one of the prime goals of the collider [9, 12, 15–43] (including the Large Hadron Collider (LHC) [44]) and non-collider [45, 46] experiments. The ongoing consistency of the LHC data with SM predictions is putting significant pressure on the simplest extra-dimensional scenarios, which are highly predictive. Some of these scenarios have been completely ruled out, including the minimal version of the Universal Extra-Dimension (mUED) model [47]. In light of the exclusion of mUED, attention turns to non-minimal [47–53] and next-to-minimal [54–62] scenarios<sup>3</sup>. Here, we are interested in a specific next-to-minimal version of the UED scenario, namely the 'fat-brane' realization of UED. In addition to the usual  $\text{TeV}^{-1}$  size extra dimension(s) (universally accessible to all SM fields and the gravity) of UED scenarios, the fat-brane realization of UED includes large ( $\sim \text{eV}^{-1}$  to  $\text{keV}^{-1}$  size) extra dimension(s) (accessible only to the gravity).

The simplest version of the UED scenario is characterized by a single flat universal (accessible to all the SM particles) extra dimension ( $y$ ), compactified on a  $S_1/Z_2$  orbifold with a radius  $R$ , known as *One Universal Extra-Dimension (OneUED)* model. The particle spectrum of *oneUED* contains infinite towers of Kaluza-Klein (KK) modes (identified by an integer  $n$ , called the KK-number) for each of the SM fields. The zero modes are identified as the corresponding SM particles. From a 4-dimensional perspective, the conservation of the momentum along the fifth direction implies the conservation of the KK-number. However, the additional  $Z_2$  symmetry ( $y \leftrightarrow -y$ ), required to obtain the chiral structure of the SM fermions, breaks the translational invariance along the 5<sup>th</sup> dimension. As a result, KK-number conservation breaks down at the loop level, leaving behind only a conserved KK-parity, defined as  $(-1)^n$ , which is an automatic outcome of the  $S_1/Z_2$  orbifolding and

---

<sup>1</sup>Arkani-Hamed, Dimopoulos, and Dvali

<sup>2</sup>Randall and Sundrum

<sup>3</sup>Non-minimal setups maintain identical gauge/Lorentz symmetry and field content as mUED but introduce non-vanishing boundary localized terms at the cut-off scale ( $\Lambda$ ). Next-to-minimal UED scenarios, on the other hand, deviate from mUED by featuring different gauge/Lorentz symmetry or field content.

has several consequences, including some exciting ones like the stability of the lightest KK particle (LKP) which can be a good candidate for cold dark matter (CDM) [10, 11, 63–71]. *OneUED*, being a higher dimensional theory, is non-renormalizable and should be treated as an effective theory valid up to a cut-off scale  $\Lambda$ . Apart from the usual SM kinetic, Yukawa, and scalar potential terms for the 5D fields, the *oneUED* Lagrangian also includes additional SM gauge and Lorentz invariant terms like the vector-like bulk mass terms [25, 26, 72–74] for the 5D fermions and kinetic (and Yukawa) terms (boundary localized terms (BLTs)) for all the 5D fields at the orbifold fixed points, *i.e.*, the boundaries of the bulk and the brane [75, 76]. In the *minimal* version of *oneUED* (*mUED* [77]), all BLTs are assumed to vanish at the cut-off scale ( $\Lambda$ ) and are radiatively generated at the low scale, which ultimately appears as corrections to the masses of the KK particles. The phenomenology of *mUED* [9, 78] is determined by only two additional parameters, namely,  $R$  and  $\Lambda$ . Hence, its predictions are precise and easily testable in different experiments. A recent study [47] on the consistency of *mUED* scenario with the DM relic density (RD) as well as collider experiments, concluded that the region of  $R^{-1}$ - $\Lambda R$  plane, which is consistent with WMAP/PLANCK measured RD [79, 80], has already been ruled out by the ATLAS multijet +  $E_T$  searches [2]. Present status of *mUED* naturally motivates several variants of UED beyond the minimal one, namely the non-minimal UED (*nmUED*) model [47], the ‘fat-brane’ realization of UED [54–62], etc. While the additional parameters (couplings associated with the non-vanishing BLTs) help reconcile the tension between the dark matter relic density and the LHC results in the case of the former, the decay of the LKP via gravity-matter interactions removes the constraints from the WMAP/PLANCK measurement of DM RD in the case of the latter.

The ‘fat-brane’ realization of UED (FB-mUED)[54–62] represents an intriguing extension of the ADD scenario. In this framework, SM particles are confined to a  $(3+m)$ -brane, which denotes a  $(3+m+1)$ -dimensional manifold embedded in a  $(4+N)$ -dimensional bulk [55, 56]. Given that  $m$  spatial dimensions are compact, the effective 4-dimensional theory encompasses KK excitations of SM fields. The dimensions of the  $m$  spatial dimensions within the bulk are restricted by the constraints set by the experimental lower limit on KK-mode masses. The term ‘fat-brane’ is derived from the fact that these  $m$  small spatial dimensions, accessible to both matter and gravity, can be analogized to the thickness of the SM 3-brane in the  $(4+N)$ -dimensional bulk [54, 57–59, 62]. In this context, gravity spans across  $N$  large extra dimensions with a size around  $\text{eV}^{-1}$ , while the propagation of matter is confined to a small length scale (approximately  $\text{TeV}^{-1}$ ), corresponding to the thickness of the SM 3-brane along these extra dimensions. In this work, we focus on the collider signatures, particularly those at the LHC, of the fat brane realization of the minimal Universal Extra-Dimension (mUED) model. The collider signatures of the fat brane realization of mUED are very different from those of the standard mUED model. While the pair production and decay of level-1 KK excitations in mUED typically result in soft leptons and jets along with missing transverse energy, the gravity-mediated decays of KK particles in the fat brane realization of mUED lead to the production of hard photons, jets, Z/W bosons, top quarks, etc. at the LHC. Therefore, the search strategies proposed for mUED in the literature are not applicable to the fat brane realization of mUED. However, supersymmetric (SUSY) scenarios with gauge-mediated supersymmetry breaking (GMSB)

[81–90], where SUSY particles decay into gravitinos alongside the corresponding SM particles, produce final state signatures similar to those of the fat brane realization of mUED. Consequently, LHC searches for GMSB signatures can indirectly help constrain the parameter space of the fat brane realization of mUED. It is important to note that while the final state signatures of GMSB and the fat brane realization of mUED are similar, the kinematics of gravity-mediated decays differ. In contrast to GMSB, which contains a single gravitino, in the fat brane mUED, there is a tower of graviton excitations. Therefore, LHC bounds on SUSY particles in GMSB are not directly applicable to the level-1 KK excitations of fat brane mUED. However, model-independent bounds on the visible cross-sections of final state signatures, such as mono-photon, di-photon, and multi-jet events associated with large missing transverse energy, can be used to derive constraints on the parameter space of the fat brane realization of mUED. In this work, we obtain the most updated bounds from the LHC searches.

The persistent consistency of LHC searches with SM background predictions has raised the mass threshold for strongly interacting BSM particles to above a few TeV. Decays of such massive BSM resonances into SM particles result in highly boosted W/Z bosons, Higgs bosons, or top quarks in the final state. Recently, tagging hadronically decaying boosted W/Z or Higgs bosons or top quarks and using them for event selection at the LHC has gained popularity. This approach offers several advantages, such as larger hadronic branching ratios, leading to higher signal rates, suppression of the QCD background due to tagging, and the possibility of kinematic reconstruction because of the absence of missing transverse energy in the final state. After establishing bounds on the level-1 KK particles in FB-mUED from existing LHC searches, we propose new search strategies involving boosted tagged hadronically decaying W/Z/H bosons or top quarks optimized for detecting level-1 KK particles in FB-mUED in future LHC runs.

The rest of the paper is organized as follows: Section 2 provides a brief overview of the fat-brane realization of mUED. Section 3 contains the key findings of our analysis. In Section 3.1 and 3.2, we discuss the KK-number conserving and gravity-mediated decays of the level-1 KK particles, respectively. In Section 3.3, we discuss the collider signatures of the fat-brane mUED scenario. In Section 3.4, we present the bounds on the model parameter space from three existing ATLAS analyses. In Section 3.5, we propose a novel analysis strategy to constrain the parameter space even further during future runs of the LHC. Finally, Section 4 concludes the paper with a summary of our findings and a discussion of potential future directions.

## 2 The fat brane realization of mUED scenario

In this work, we focus on the phenomenology of the fat brane realization of the minimal Universal Extra Dimensions (mUED) scenario. In this framework, all the SM fields are allowed to propagate in one small, compactified extra dimension ( $y$ ), which is embedded in a  $(4 + N)$ -dimensional bulk fully accessible only to gravity. Embedding the mUED scenario into a gravity-accessible  $(4 + N)$ -dimensional bulk leads to gravity-matter interactions, which

allow gravity-mediated decays for the KK particles. The theoretical structure of mUED has already been briefly discussed in the introduction. For a detailed discussion on the KK decomposition of SM fields in five dimensions on the  $S^1/Z_2$  orbifold and the resulting effective four-dimensional Lagrangian, please refer to Ref. [9, 77, 78]. The phenomenology of mUED has been discussed in Ref. [31, 36, 40, 42, 91–93]. The fat brane realization of mUED and the consequences of gravity-matter interactions have been studied in Ref. [54–62]. However, for the sake of completeness, we provide a brief introduction to the gravity-matter interaction in the framework of fat brane realization of mUED in the following.

## 2.1 Matter-Gravity Interaction

In the fat-brane scenario, gravity is permitted to propagate into  $N$  large extra dimensions, which are subsequently compactified on an  $N$ -dimensional torus  $T^N$  with a volume  $V_N \sim r^N$ , where  $r$  represents the size of the  $N$  large extra dimensions. The 4D Planck mass  $M_{\text{Pl}}$  can be derived from the fundamental  $(4 + N)$ -dimensional Planck mass  $M_D$  as:

$$M_{\text{Pl}}^2 = M_D^{N+2} \left( \frac{r}{2\pi} \right)^N.$$

Assuming there are  $N$  such large extra dimensions denoted by  $x^5, \dots, x^{4+N}$  with a common size of  $r \sim \text{eV}^{-1}$ , and one small extra dimension denoted by  $y = x^4$  with a size of  $\text{TeV}^{-1}$ , one can express the interaction of SM fields and the graviton in the higher dimension as:

$$S_{\text{int}} = \int dx^{4+N} \delta(x^5) \dots \delta(x^{4+N}) \sqrt{-\hat{g}} \mathcal{L}_m,$$

where  $\mathcal{L}_m$  represents the Lagrangian density for SM fermions, gauge bosons, and the Higgs. The higher dimensional flat metric  $\hat{g}$  can be expressed as  $\hat{g}_{\hat{\mu}\hat{\nu}} = \eta_{\hat{\mu}\hat{\nu}} + \hat{k} \hat{h}_{\hat{\mu}\hat{\nu}}$ . The hat denotes quantities that live in  $(4 + N)$  dimensions, i.e.,  $\hat{\mu}, \hat{\nu} = 0, 1, 2, 3, 5, \dots, 4 + N$ . Here  $\hat{k}^2 = 16\pi G^{4+N}$  with  $G^{4+N}$  being the gravitational constant in  $(4 + N)$  dimensions. The KK-decomposition of the  $(4 + N)$  dimensional graviton field  $\hat{h}_{\hat{\mu}\hat{\nu}}$  can be written as,

$$\hat{h}_{\hat{\mu}\hat{\nu}}(x, y) = \sum_{\vec{n}} \hat{h}_{\hat{\mu}\hat{\nu}}^{\vec{n}}(x) \exp\left(i \frac{2\pi \vec{n} \cdot \vec{y}}{r}\right), \quad (2.1)$$

where  $\hat{h}_{\hat{\mu}\hat{\nu}}^{\vec{n}}(x)$  is the  $\vec{n}^{\text{th}}$  KK-excitation of the graviton field with  $\vec{n} = \{n_5, \dots, n_{4+N}\}$  being the KK-number representing the  $\vec{n}^{\text{th}}$  KK-excitation. The  $\vec{n}^{\text{th}}$  KK-excitation of the graviton field,  $\hat{h}_{\hat{\mu}\hat{\nu}}^{\vec{n}}(x)$ , can be decomposed into a four-dimensional tensor  $h_{\mu\nu}^{\vec{n}}$  (the graviton),  $N$  vectors  $A_{\mu i}^{\vec{n}}$  (the graviphotons), and  $N^2$  scalar fields  $\phi_{ij}^{\vec{n}}$  (the graviscalars) as,

$$\hat{h}_{\hat{\mu}\hat{\nu}}^{\vec{n}} = V_N^{-1/2} \begin{pmatrix} h_{\mu\nu}^{\vec{n}} + \eta_{\mu\nu} \phi^{\vec{n}} & A_{\mu i}^{\vec{n}} \\ A_{\nu j}^{\vec{n}} & 2\phi_{i,j}^{\vec{n}} \end{pmatrix} \quad (2.2)$$

where  $V_N$  is the volume of the  $N$  dimensional torus,  $i, j = 5, 6, \dots, (4 + N)$ , and  $\phi^{\vec{n}} = \phi_{ii}^{\vec{n}}$ . All the  $\frac{(N+4)(N+5)}{2}$  components of the symmetric  $(N + 4)$  dimensional rank-2 tensor,  $\hat{h}_{\hat{\mu}\hat{\nu}}^{\vec{n}}(x)$ , are not independent. In order to eliminate the unphysical degrees of freedom, one has to make particular gauge choices, which have been done in [94–97] and discussed briefly in the

following. The de Donder condition  $\partial^{\hat{\mu}} \left( \hat{h}_{\hat{\mu}\hat{\nu}} - \frac{1}{2} \eta_{\hat{\mu}\hat{\nu}} \hat{h} \right) = 0$ , where  $\hat{h} = \hat{h}_{\hat{\mu}}^{\hat{\mu}}$ , in addition with the gauge conditions,  $n_i A_{\mu i}^{\vec{n}} = 0$ ,  $n_i \phi_{ij}^{\vec{n}} = 0$ , eliminate  $2(N+4)$  spurious degrees of freedom leaving  $\frac{(N+4)(N+1)}{2}$  physical degrees of freedom at level  $\vec{n}$ , associated with a massive spin-2 graviton  $\tilde{h}_{\mu\nu}^{\vec{n}}$  (5 degrees of freedom),  $N-1$  massive vector bosons  $\tilde{A}_{\mu i}^{\vec{n}}$  ( $3 \times (N-1)$  degrees of freedom) known as graviphotons, plus  $\frac{N(N-1)}{2}$  massive scalars  $\tilde{\phi}_{ij}^{\vec{n}}$  known as graviscalars with 1 degree of freedom each:

$$\begin{aligned}\tilde{h}_{\mu\nu}^{\vec{n}} &= h_{\mu\nu}^{\vec{n}} - \omega \left( \frac{\partial_\mu \partial_\nu}{m_{\vec{n}}^2} - \frac{1}{2} \eta_{\mu\nu} \right) \tilde{\phi}^{\vec{n}}, \\ \tilde{A}_{\mu i}^{\vec{n}} &= A_{\mu i}^{\vec{n}}, \\ \frac{1}{\sqrt{2}} \tilde{\phi}_{ij}^{\vec{n}} &= \phi_{ij}^{\vec{n}} + \frac{3\omega a}{2} \left( \delta_{ij} - \frac{n_i n_j}{\vec{n}^2} \right) \tilde{\phi}^{\vec{n}}\end{aligned}\tag{2.3}$$

where  $\tilde{\phi}^{\vec{n}} = 2\phi_{ii}^{\vec{n}}/(3\omega)$ ,  $\omega = \sqrt{2/(3N+6)}$  and  $a$  satisfies  $3(N-1)a^2 + 6a - 1 = 0$ . For a given  $\vec{n}$  all the gravity excitations (graviton, graviphotons, or graviscalars) share the common mass  $m_{\vec{n}} = 2\pi|\vec{n}|/r$ .

The  $(4+N)$  dimensional action representing the gravity-matter interaction is given by,

$$S_{\text{int}} = -\frac{\hat{k}}{2} \int d^{N+4}x \delta(x^5) \dots \delta(x^N) \hat{h}^{\hat{\mu}\hat{\nu}} T_{\hat{\mu}\hat{\nu}},\tag{2.4}$$

where  $\hat{k} = V_N^{1/2} \sqrt{16\pi G_N^4}$  is the  $(4+N)$  dimensional gravitational coupling and  $T_{\hat{\mu}\hat{\nu}}$  is the energy-momentum tensor, which in terms of the matter Lagrangian  $\mathcal{L}_m$  has the following form,

$$T_{\hat{\mu}\hat{\nu}} = \left( -\hat{\eta}_{\hat{\mu}\hat{\nu}} + 2 \frac{d\mathcal{L}_m}{d\hat{g}^{\hat{\mu}\hat{\nu}}} \right)_{\hat{g}=\hat{\eta}}\tag{2.5}$$

Following equation 2.1 and 2.5, we can express the gravity-matter action in terms of the KK modes of the physical gravity field,

$$\begin{aligned}S_{\text{int}} &= -\frac{k}{2} \int d^4x \sum_n \left\{ \left[ \tilde{h}_{\mu\nu}^{\vec{n}} + \omega \left( \eta_{\mu\nu} + \frac{\partial_\mu \partial_\nu}{m_{\vec{n}}^2} \right) \tilde{\phi}^{\vec{n}} \right] T_{n_5}^{\mu\nu} \right. \\ &\quad \left. - 2\tilde{A}_{\mu 5}^{\vec{n}} T_{n_5 5}^\mu + \left( \sqrt{2} \tilde{\phi}_{55}^{\vec{n}} - 3\omega a \left( 1 - \frac{n_5^2}{\vec{n}^2} \right) \tilde{\phi}^{\vec{n}} \right) T_{55}^{n_5} \right\}\end{aligned}\tag{2.6}$$

Where we have defined,

$$T_{MN}^{n_5}(x) = \int_0^{\pi R} dy T_{MN}(x, y) e^{\frac{2\pi i n_5 y}{r}}\tag{2.7}$$

Using equation 2.6, it is straightforward to calculate the Feynman rules for gravity-matter interactions. The resulting expressions are lengthy. We redirect the readers to [96] for a detailed discussion.

---

<sup>4</sup>Here  $G_N$  is the Universal Gravitational Constant

### 3 Collider Phenomenology

After briefly introducing the model and the gravity-matter interactions for the KK particles, we are now equipped to discuss the collider signatures of this model. Due to the conservation of KK-parity, the level-1 KK-particles (which are odd under KK-parity) can only be pair-produced at the LHC. The particle spectrum of level-1 KK fields includes excited fermions ( $SU(2)_L$ -doublets:  $Q_1$  and  $L_1$ ;  $SU(2)_L$ -singlets:  $u_1$ ,  $d_1$ , and  $e_1$ ), Higgses, and gauge bosons (excited gluon:  $g_1$ , W-boson:  $W_1^\pm$ , Z-boson:  $Z_1$ , and photon:  $\gamma_1$ ). The pair production of the level-1 KK-quarks/gluons, being driven by QCD processes, has the highest production cross-sections among the level-1 KK particles. KK-parity forbids the decay of the level-1 KK-particles completely into SM particles (which are even under KK-parity). In the framework of the fat-brane realization of mUED, the decays of the level-1 KK-particles can be categorized into two categories: **Category I:** The level-1 KK-particles can decay into lighter level-1 KK-particles in association with one or more SM particles. These decays are KK-number conserving, and hence, we will denote these decays as KKNC decays for the rest of the article. In the absence of any kinematically allowed KKNC decay modes for the lightest level-1 particle, the KKNC decay for the lightest level-1 particle is forbidden. **Category II:** In the presence of gravity-matter interaction, the level-1 KK particles can also decay into lighter gravity excitations (KK graviton, graviphoton, or graviscalars) in association with the corresponding SM particles. For the rest of the article, we denote these decays as gravity-mediated decays (GMD). The collider signatures of the level-1 KK-particles in the framework of the fat-brane realization of mUED crucially depend on the decays of the level-1 KK-particles, which will be discussed in the following.

#### 3.1 KK-Number Conserving (KKNC) Decays

The KK parity allows the decay of level-1 KK particles into lighter level-1 KK particles. Therefore, the mass spectrum of level-1 KK particles plays a crucial role in determining the decay of these particles. In the absence of electroweak symmetry breaking, the masses of all level-1 KK particles are given by  $R^{-1}$ . However, radiative corrections [77] remove this degeneracy. KK-fermions receive positive mass corrections from both gauge interactions (with KK-gauge bosons) and Yukawa interactions. The gauge fields receive mass corrections from self-interactions and gauge interactions (with KK-fermions). Gauge interactions give a negative mass shift, while self-interactions give a positive mass shift. However, the mass of the hypercharge gauge boson ( $\gamma_1$ ) receives only negative corrections from fermionic loops. Numerical computations show that the lightest KK particle is the hypercharge gauge boson  $\gamma_1$ , and the heaviest level-1 KK particle is the excited gluon ( $g_1$ ), followed by the excited quarks, level-1 electroweak gauge bosons, and leptons. The radiative corrections are proportional to  $\ln(\Lambda^2/\mu^2)$ , where  $\Lambda$  is the cutoff scale. The perturbativity of the  $U(1)_Y$  gauge coupling requires  $\Lambda \leq 40R^{-1}$ . However, much stronger bounds arise from the running of the Higgs-boson self-coupling and the stability of the electroweak vacuum [98, 99]. Throughout this analysis, we choose  $\Lambda = 5R^{-1}$ .

For fixed  $R^{-1}$  and  $\Lambda$ ,  $g_1$ , being the heaviest particle in the spectrum, can decay into doublet  $Q_1$  and singlet ( $u_1, d_1$ ) quarks with almost equal branching fractions. The singlet



quarks can only decay into  $\gamma_1$  and an SM quark. On the other hand, the doublet quarks can mostly decay into level-1 KK electroweak gauge bosons, namely  $Z_1$  and  $W_1$ . The hadronic decays of  $W_1$  and  $Z_1$  are kinematically closed. Therefore, they can only decay into level-1 KK leptons and the corresponding SM lepton. These level-1 leptons then decay into SM leptons and  $\gamma_1$ . Being the lightest level-1 KK particle,  $\gamma_1$  does not have any KKNC decay. Note that the masses and the KKNC decay widths of level-1 particles do not depend on the number of large extra dimensions,  $N$ , and are determined only by the size of the small extra dimension  $R^{-1}$  and the cutoff scale of the model  $\Lambda$ .

### 3.2 Gravity Mediated Decays (GMD)

In the fat-brane scenario, the matter fields are confined to a small distance along the fifth dimension. This results in breaking translation invariance along the fifth dimension at the boundaries  $y = 0$  and  $y = \pi R$ . Consequently, the interaction between gravity and matter does not respect KK number conservation, and the KK excitations of SM particles can decay directly into the corresponding SM particles with the emission of a gravity excitation. The gravity-mediated decay widths of the level-1 KK particles are discussed in detail in [94, 96], and for the sake of completeness, we summarize their results in Appendix A.1. The decay width into individual graviton modes is suppressed by a factor of  $1/M_{\text{Pl}}^2$  and hence is negligible. However, each matter field can decay into any kinematically allowed gravity excitation. Since the mass difference between individual gravity excitations is of the order  $eV^{-1}$ , the number of allowed gravity-mediated decay modes is large. Ergo, the GMD width of the matter fields can be significant and compete with the corresponding KKNC decay width. The total decay width can be expressed as the sum of widths into individual gravity excitations, i.e.,

$$\Gamma = \sum_{\vec{n}} \Gamma_{\vec{n}} = \sum \Gamma_{h\vec{n}} + \Gamma_{A\vec{n}} + \Gamma_{\phi\vec{n}} \quad (3.1)$$

Since the mass difference between individual gravity excitations is almost negligible, the sum can be replaced by an integral over the graviton density of states (see [100]), i.e.,

$$\Gamma = \frac{M_{\text{Pl}}^2}{M_D^{N+2}} \int dm d\Omega \Gamma_{\vec{n}} m_{\vec{n}}^{N-1} \quad (3.2)$$

where  $M_{\text{Pl}}$  is the four-dimensional Planck mass,  $M_D$  is the fundamental Planck mass, and  $m_{\vec{n}}$  is the mass of the level  $\vec{n}$  gravity excitation. Figure 1 shows the normalized gravity-mediated partial widths of a level-1 KK-gluon as a function of the masses of the gravity excitations for three different values of  $N$ . In Figure 1, we have assumed  $R^{-1} = 500$  GeV. For  $N = 2$ , the light gravity modes mostly contribute, while for  $N = 6$ , the massive gravitons dominate the decay width.

### 3.3 Collider Signatures

Level-1 KK particles, after being pair-produced at colliders, can decay via KKNC or gravity-mediated processes. While KKNC decays result in relatively soft <sup>5</sup> jets and leptons, gravity-

---

<sup>5</sup>The KKNC decays allow heavier level-1 KK particles to decay into lighter level-1 KK particles in association with one or more SM quarks or leptons. The hardness of the SM quarks/leptons depends on

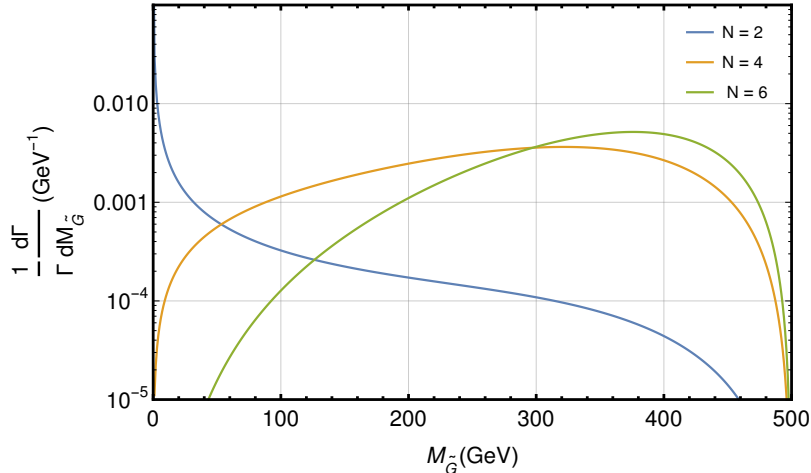


**Figure 1:** The normalized partial decay width for level-1 KK-gluon into a gluon and gravity excitations as a function of the mass of the gravity excitations, for  $R^{-1} = 500$  GeV and  $M_D = 5$  TeV.

mediated decays produce hard <sup>6</sup> jets, leptons, photons, and high- $p_T$  massive SM bosons (W/Z/Higgs bosons) or top quarks. Therefore, the collider signature of the fat brane minimal Universal Extra Dimensions (mUED) scenario crucially depends on the relative strengths of KKNC decays and gravity-mediated decays.

The KKNC decays are determined by SM parameters as well as the masses and mass-splitting between the KK particles, which are controlled by the radius of compactification of the small extra dimension,  $R$ , and the cut-off scale,  $\Lambda$ . On the other hand, the gravity-mediated decay widths depend on the masses of the KK particles as well as the fundamental  $(4+N)$ -dimensional Planck mass,  $M_D$ , and the number of large extra dimensions,  $N$ . For a fixed cut-off scale  $\Lambda = 5R^{-1}$ , the branching ratios of gravity-mediated decays and KKNC decays depend only on  $R^{-1}$  and  $M_D$ . In Fig. 2, we present the branching ratios for the gravity-mediated decays of the level-1 KK-gluons (indicated by the color gradient) on the  $R^{-1}$ - $M_D$  plane for three different values of the number of large extra dimensions:  $N = 2$  (top left panel),  $N = 4$  (top right panel), and  $N = 6$  (bottom panel). Fig. 2 shows that for  $N = 2$ , gravity-mediated decays dominate over almost the entire  $R^{-1}$ - $M_D$  plane, while for  $N = 6$ , KKNC decays become more significant. The different possible final state signatures resulting from the pair production of level-1 quarks/gluons at the LHC are summarized in the following.

---

the mass splitting between the parent and daughter level-1 KK particles. Due to the small mass splitting between level-1 KK particles resulting from radiative corrections, the final state resulting from the KKNC decays typically features soft jets and leptons.

<sup>6</sup>Gravity-mediated processes allow level-1 KK particles to decay into a gravity excitation accompanied by the corresponding SM particle. The gravity excitations, resulting from the compactification of the large extra dimensions, can have a significant mass difference compared to the level-1 KK particles. Consequently, the SM jets, leptons, photons, W/Z/Higgs bosons, and top quarks, produced from the decays of level-1 light quarks/gluons, leptons, W/Z/Higgs bosons, and top quarks, respectively, are usually energetic.

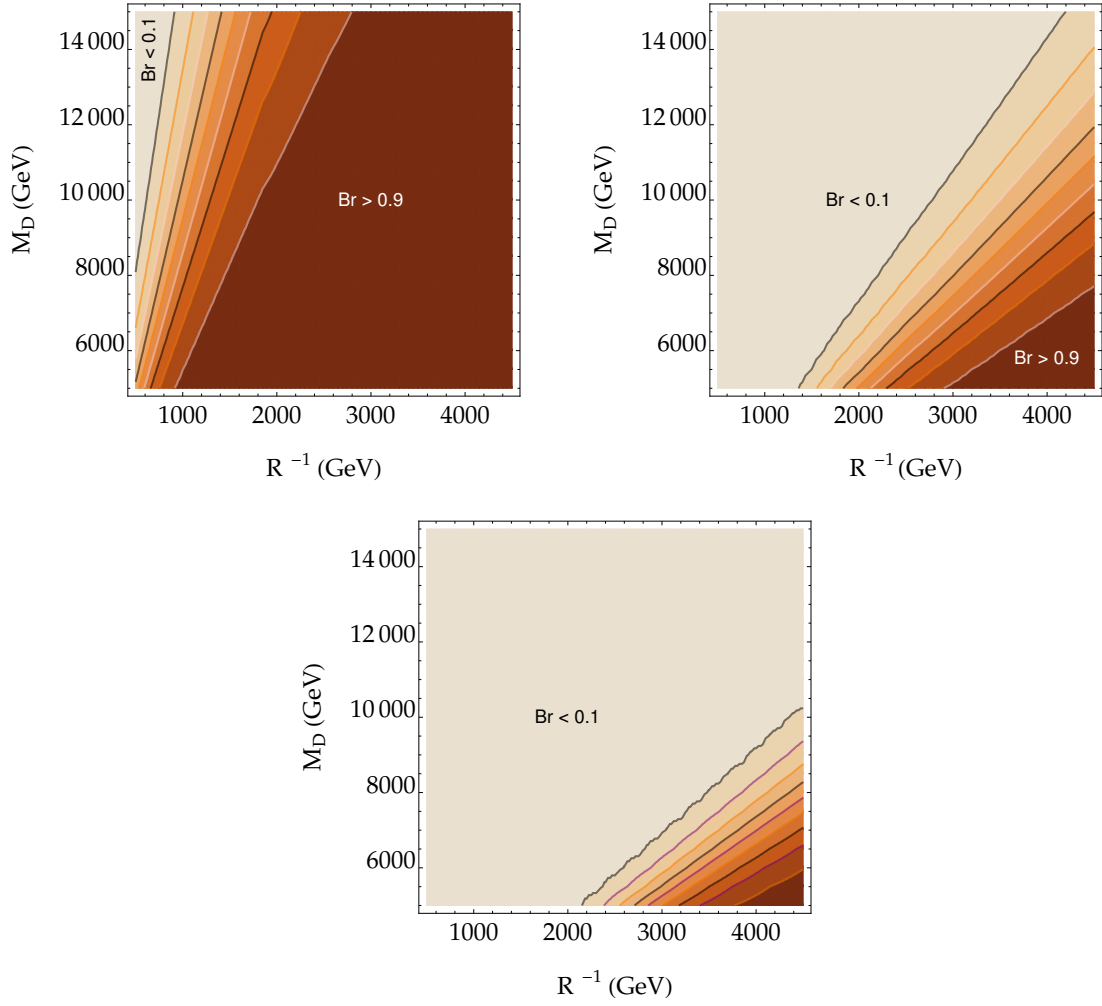


**Figure 2:** The branching ratios for the gravity-mediated decays of the level-1 KK-gluons (indicated by the color gradient) on the  $R^{-1}$ - $M_D$  plane for three different values of the number of large extra dimensions:  $N = 2$  (top left panel),  $N = 4$  (top right panel), and  $N = 6$  (bottom panel).

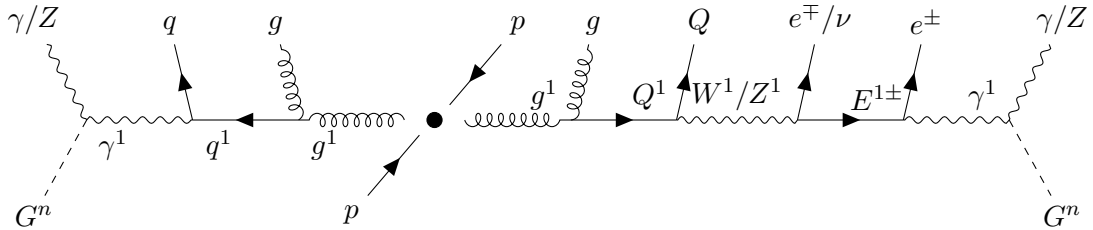


**Figure 3:** Schematic Feynman diagram for  $pp \rightarrow g^1 g^1$  and its subsequent decays in the scenario when KKNC decays dominate.

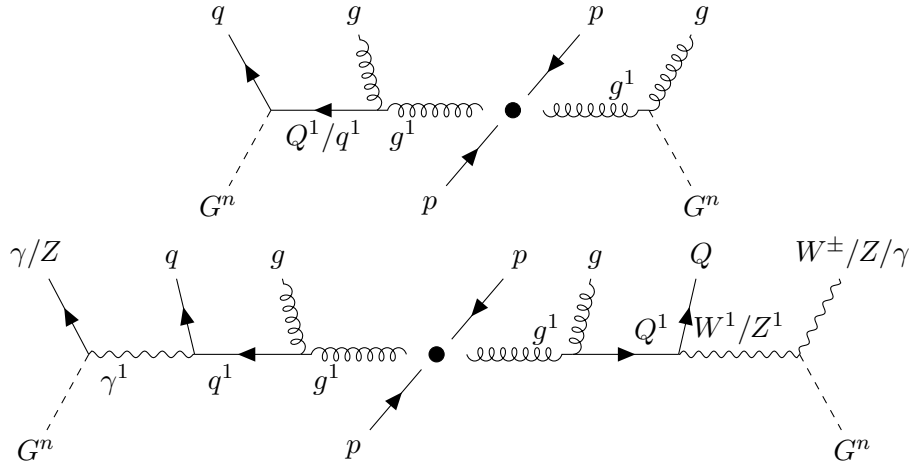


**Figure 4:** Schematic Feynman diagram for  $pp \rightarrow g^1 g^1$  and subsequent decays in the scenario when GMD decays dominate.

1. **Scenarios with KKNC decays dominating over the GMDs:** In the scenario where KKNC decays dominate over gravity-mediated decays, the pair-produced level-1 KK quarks/gluons decay into the lightest level-1 KK particle, namely the level-1 KK excitation of the  $U(1)_Y$  gauge boson denoted by  $\gamma_1$ , through cascades involving other level-1 KK particles. Such decay cascades give rise to multiple quarks and leptons in the final state. In the absence of any kinematically allowed KKNC decay for the lightest level-1 KK particle,  $\gamma_1$  undergoes gravity-mediated decay into a photon or SM Z-boson in association with a gravity excitation. Therefore, in this scenario, the pair production of level-1 quarks/gluons at the LHC leads to hard photons/Z-bosons plus soft jets/leptons in association with large missing transverse energy resulting from the invisible gravity excitations. The Feynman diagram depicting the pair production and subsequent decay of level-1 gluons is presented in Fig. 3.
2. **Scenarios with GMDs dominating over the KKNC decays:** In the scenario where gravity-mediated decays dominate over KKNC decays, the pair-produced level-1 KK quarks/gluons undergo gravity-mediated decays into a gravity excitation in association with a SM quark or gluon. Therefore, the pair and associated production of level-1 KK excitations of the light SM quarks and gluons at the LHC gives rise to hard jets and a large missing transverse energy (resulting from the invisible gravity excitations) signature. On the other hand, the pair production of level-1 top quarks results in boosted top quarks plus missing transverse energy in the final state. The Feynman diagram in Fig. 4 (top panel) schematically shows the production and possible decays of level-1 gluons.
3. **Scenarios with comparable gravity mediated and KKNC decay widths:** The Feynman diagram in Fig. 4 (bottom panel) schematically shows the production and possible decays of level-1 gluons in a scenario with comparable decay widths for

gravity-mediated decays (GMDs) and KKNC decays. Note that the KKNC decay widths are enhanced by color factors for the strongly interacting level-1 particles. The Feynman diagram in Fig. 4 (bottom panel) corresponds to a region of parameter space with comparable gravity-mediated and KKNC decay widths for the color singlet level-1 particles. In this case, level-1 quarks/gluons follow the KKNC decay modes, while level-1 weak gauge bosons or leptons undergo gravity-mediated decays, leading to interesting high  $p_T$  photons/massive SM gauge bosons or Higgs bosons in the final state.

To summarize the signatures of fat brane realization of mUED at the LHC, the pair and associated production of level-1 quarks/gluons at the LHC within the framework of the fat brane realization of mUED results in conventional mono-photon, di-photon, and multi-jet final states associated with large missing transverse energy. These signatures have been extensively studied by the CMS and ATLAS collaborations of the LHC in the context of different supersymmetric scenarios. Depending on the region of the  $R^{-1}$ - $M_D$  plane and the number of large extra dimensions  $N$ , the production and decay of level-1 quarks/gluons might also give rise to interesting final states with boosted (high- $p_T$ ) W/Z/Higgs bosons or top quarks. In the following, we first obtain bounds on the  $R^{-1}$ - $M_D$  plane for different values of  $N$  by recasting the LHC results from mono-photon, di-photon, and multi-jet plus large missing transverse energy searches in the context of our model. After establishing the bounds on the  $R^{-1}$ - $M_D$  plane, we focus on novel search strategies that use machine learning-based algorithms to tag boosted W/Z/Higgs bosons or top quarks. These strategies aim to suppress the SM background and thus enhance the sensitivity of future LHC runs.

### 3.4 Bounds from the existing LHC searches

Final state topologies with multiple hard photons (mono-photon or di-photon signatures) or jets (multi-jet signatures) plus large missing transverse momentum are common in various BSM scenarios, particularly in different versions of supersymmetric models. These signatures have been extensively studied by the CMS and ATLAS collaborations at the LHC. Although LHC studies are designed to search for specific BSM scenarios, the model-independent bounds on visible signal cross-sections in different signal regions can be used to constrain the parameter space of other BSM scenarios with similar signatures. In this work, we study three ATLAS searches at the 13 TeV LHC: the di-photon plus missing transverse energy search with  $36.1 \text{ fb}^{-1}$  luminosity data, the multi-jets plus missing transverse energy search, and the mono-photon plus missing transverse energy search with  $139 \text{ fb}^{-1}$  integrated luminosity data. These analyses are designed to search for SUSY particles in various SUSY scenarios. We use the model-independent bounds on visible signal cross-sections in different signal regions to constrain the  $R^{-1}$ - $M_D$  plane for different values of the number of large extra dimensions  $N$ . Before presenting the constraints on the  $R^{-1}$ - $M_D$  plane, we briefly discuss the ATLAS searches, the technical details of our implementation and validation of these searches, and the simulation of events in the framework of the fat brane mUED model.

### 3.4.1 ATLAS mono-photon plus missing transverse energy search [1]

Several experimental searches at the LHC [3, 101–104] have investigated the diphoton/mono-photon final states. In the absence of any excess over the SM background predictions, stringent constraints have been set on the model-independent visible cross-section. In this work, we use the ATLAS mono-photon search result presented in Ref. [1] to constrain the parameter space of our model. In Ref. [1], the ATLAS collaboration searched for events with at least one hard ( $p_T > 145$  GeV) photon in association with large missing transverse energy ( $E_T^{\text{miss}}$ ) in the context of SUSY scenarios with gauge-mediated SUSY breaking (GMSB). In GMSB-type SUSY scenarios with gravitino as the lightest SUSY particle (LSP), the decay of the lightest neutralino ( $\tilde{\chi}_1^0$ ), the next-to-lightest SUSY particle (NLSP), into the gravitino LSP in association with a photon or Z/Higgs boson gives rise to final states with hard photons and large  $E_T^{\text{miss}}$  resulting from the invisible gravitinos in the LHC detector.

Object Reconstruction Criteria [1]	
Object	Criteria
Photon	$p_T > 50$ GeV, $ \eta  \in [0, 1.37] \cup [1.52, 2.37]$ ; Isolation criteria [1]
Electron	$p_T > 25$ GeV, $ \eta  \in [0, 1.37] \cup [1.52, 2.47]$ ; Loose isolation criteria
Muon	$p_T > 25$ GeV, $ \eta  < 2.7$ ; Loose isolation criteria
Jet	Anti- $k_T$ algorithm [105, 106] with $R = 0.4$ , $p_T > 30$ GeV, $ \eta  < 2.5$
$E_T^{\text{miss}}$	The negative vector sum of transverse momenta of all visible objects, including the calorimeter energy deposits not matching any reconstructed objects

Object Isolation Criteria [1]	
$\gamma$ -Lepton	Photon candidates within $\Delta R_{\gamma l} < 0.4$ of a lepton are removed
e-Jet	Jets removed if an electron is within $\Delta R_{ej} < 0.2$ Electrons removed for $0.2 < \Delta R_{ej} < 0.4$
$\mu$ -Jet	Muons within $\Delta R_{\mu j} < 0.4$ of a jet are removed if the jet has at least three good-quality tracks; otherwise, the jet is removed
$\gamma$ -Jet	Jets within $\Delta R_{\gamma j} < 0.4$ of a photon are eliminated

Electron/Jets faking photon	
The possibilities of electrons and jets faking as photons are considered according to Ref. [107, 108]	

**Table 1:** Summary of object reconstruction criteria used in Ref. [1] as well as in our implementation.

As discussed in the previous section, the pair-production and decay of the level-1 KK particles in the framework of fat brane realization of mUED also give rise to similar final state topologies with photons plus  $E_T^{\text{miss}}$ . However, the kinematics for the decay of SUSY particles in GMSB and KK-particles in fat brane realization of mUED are very different. For example, while the NLSP  $\tilde{\chi}_1^0$  in the GMSB scenario decays into a single light gravitino by emitting a hard photon/Z/Higgs boson, the next-to-lightest KK particle (NLKP)  $\gamma_1$  in fat brane realization of mUED can decay into any kinematically allowed member of

the tower of gravity excitations. Therefore, the  $p_T$  spectrum of the photon or Z-boson resulting from the NLKP decay is not necessarily always very hard. As a result, the bounds obtained in Ref. [1] on the gluino-neutralino mass plane are not applicable to constrain the  $m_{g_1}-m_{\gamma_1}$  plane of fat brane mUED. However, the model-independent bounds on visible signal cross-sections in different mono-photon signal regions in Ref. [1] are applicable after proper simulation of the fat brane mUED events following the object reconstruction and event selection criteria of Ref. [1]. A detailed discussion about object reconstruction, event selection, and mono-photon signal region definitions, which we have implemented in our event simulation, can be found in Ref. [1] and is also tabulated in Table 1 and 2. Tables 1 and 2 provide a summary of the criteria used in our analysis, as implemented by the ATLAS collaboration. Table 1 details the object reconstruction and isolation criteria for different physics objects, while Table 2 outlines the criteria for the three signal regions, SRL, SRM, and SRH, used to probe different areas of the gluino- $\tilde{\chi}_1^0$  mass plane in GMSB in Ref. [1]. In our analysis, we have used the model-independent bounds presented in Table 2 on the visible signal cross-section in the signal regions SRL, SRM, and SRH to constrain the parameter space of the fat-brane realization of mUED. The implementation of object reconstruction criteria in Table 1, and signal region definition in Table 2, as well as the validation of our implementation, are discussed in the following.

	SRL	SRM	SRH
$N_{photons}$	$\geq 1$	$\geq 1$	$\geq 1$
$p_T^{leading-\gamma}$	$> 145 \text{ GeV}$	$> 300 \text{ GeV}$	$> 400 \text{ GeV}$
$N_{leptons}$	0	0	0
$N_{jets}$	$\geq 5$	$\geq 5$	$\geq 3$
$\Delta\phi(jet, E_T^{miss})$	$> 0.4$	$> 0.4$	$> 0.4$
$\Delta\phi(\gamma, E_T^{miss})$	$> 0.4$	$> 0.4$	$> 0.4$
$E_T^{miss}$	$> 250 \text{ GeV}$	$> 300 \text{ GeV}$	$> 600 \text{ GeV}$
$H_T$	$> 2000 \text{ GeV}$	$> 1600 \text{ GeV}$	$> 1600 \text{ GeV}$
$R_T^4$	$< 0.90$	$< 0.90$	-
$\langle\epsilon\sigma\rangle_{obs}^{95} \text{ (fb)}$	0.034	0.022	0.054

**Table 2:** Cuts used by the ATLAS collaboration to define the three signal regions along with the model-independent 95 % Confidence Level upper bound on the visible cross-section. Here,  $H_T$  represents the scalar sum of the transverse momentum of all signal region jets and the leading photon, while  $R_T^4$  represents the ratio of the scalar sum of the transverse momentum of the four leading signal region jets to the scalar sum of the transverse momentum of all signal region jets in the event. The other symbols carry their usual meaning.

**Implementation & Validation:** The results of the mono-photon plus  $E_T^{miss}$  analysis in Ref. [1] are interpreted as bounds on the gluino NLSP-neutralino mass plane in the context of a simplified GMSB scenario. To validate our implementation of the object reconstruction

and event selection procedure described in Ref. [1], we reproduced the cut-flow tables from Ref. [1] for a given set of parameters of the simplified GMSB scenario<sup>7</sup>. We used the default minimal supersymmetric standard model (MSSM) file provided with SARAH [109] and generated the particle spectrum and decay tables in SPheno [110]. Gluino pairs with up to two additional partons were generated in MG5\_AMC@NLO [111], and their subsequent decays, showering, and hadronization were simulated in PYTHIA8 [112]. The gravitino decay modes of supersymmetric particles were implemented in the PYTHIA code using the analytical partial decay width expressions from Refs. [113, 114]. Reconstruction of different physics objects was performed in the fast detector simulator DELPHES [115] using the prescription discussed in Section 3.4.1. To validate our implementation, we replicated the cut-flow table found in HEPData [1]. The outcome for the signal region SRL is provided in Table 3. Similar results were obtained for the SRM and SRH signal regions, and we present them in Appendix A.2. In Table 3, we present our simulation results alongside those of the ATLAS collaboration in Ref. [1] to facilitate comparison, and there is a notable concurrence between the two sets of numbers.

### 3.4.2 ATLAS multi-jet plus missing transverse energy search [2]

The fat-brane realization of the mUED model can lead to final states with multiple hard jets and large missing transverse momentum when gravity-mediated decays dominate over the KKNC decay for level-1 quarks/gluons. In such scenarios, pair-produced level-1 quarks/gluons directly decay to a graviton excitation in association with an SM quark/gluon, giving rise to multiple hard jets at the LHC. Multi-jets plus  $E_T^{\text{miss}}$  final states have been extensively searched at the LHC [2, 116–121] as a signature of different BSM scenarios. We have considered the recent multi-jet search by the ATLAS collaboration in Ref. [2] with the full ( $139 \text{ fb}^{-1}$  integrated luminosity) run-II data of the LHC at 13 TeV center-of-mass energy. Although the analysis in Ref. [2] is dedicated to the search for squarks and gluinos in the context of supersymmetry, the model-independent 95% CL upper limits on the visible  $n_j + E_T^{\text{miss}}$  cross-sections ( $\langle\sigma\rangle_{95}^{\text{obs}}$ ) for different signal regions (SRs) can be used to constrain the parameter space of other BSM scenarios like our scenario, which also gives rise to similar final states. In Ref. [2], the ATLAS collaboration defined ten signal regions for their model-independent study of multijet plus missing transverse energy final states. The signal regions are defined by varying numbers of jet multiplicities (between 2–6) along with the

---

<sup>7</sup>While reproducing the limits and cut-flow tables in Ref. [1], we identified several simplified assumptions adopted in Ref. [1] that are not theoretically consistent. These assumptions lead to bounds on the gluino NLSP-neutralino mass plane that should be interpreted cautiously. For example, Ref. [1] considers the pair production and SUSY cascade decays of gluinos to the neutralino NLSP, followed by gravity-mediated decays of the NLSP to a gravitino in association with a photon or a Z/Higgs boson. However, we found that, for the given set of parameters, the gravity-mediated decays of different SUSY particles in the cascade, which were neglected in Ref. [1], can be significant in different regions of the gluino NLSP-neutralino mass plane. This allows particles to decay into gravitinos instead of lighter SUSY particles in the cascade, leading to a reduced cross-section for the signal regions defined in Ref. [1]. Obtaining a realistic bound on the gluino NLSP-neutralino mass plane, considering all possible complexities associated with the decays of SUSY particles in the cascade is beyond the scope of this article. We plan to address these issues in a separate publication.



Cuts	$m_{\tilde{g}} = 2000\text{GeV}, m_{\tilde{\chi}_1^0} = 250\text{GeV}$			
	$\gamma/Z$		$\gamma/h$	
	Hepdata	Our Result	Hepdata	Our Result
Trigger (one photon $p_T > 140$ Gev)	47.26	49.07	49.12	46.21
At least one photon	47.19	49.07	49.02	46.21
Lepton Veto	29.80	31.97	33.36	33.07
Leading photon $p_T > 145$ Gev	26.42	31.49	30.54	32.56
$E_T^{miss} > 250$ Gev	18.96	21.28	21.18	21.89
Number of Jets $\geq 5$	18.65	21.21	20.82	21.78
$\Delta\phi(jet, E_T^{miss}) > 0.4$	15.86	17.68	17.65	17.59
$\Delta\phi(\gamma, E_T^{miss}) > 0.4$	12.04	13.94	13.51	14.10
$H_T > 2000$ GeV	10.27	10.87	11.77	11.19
$R_T^4 < 0.9$	8.08	9.52	9.40	9.61

**Table 3:** Cut-Flow table for the SRL signal region. The entries in the second and fourth columns are the results provided by the ATLAS collaboration [1] in the form of Hepdata. The entries in the third and fifth columns represent our simulated results.

minimum value of the effective mass  $m_{\text{eff}}$ . In view of the high level of agreement between the predicted background and observed yield in all signal regions, a model-independent 95% CL upper limit is set on the visible BSM contribution to the multijet cross-section ( $\langle\sigma\rangle_{95}^{\text{obs}}$ ) for each signal region. In our analysis, we have used the ATLAS-derived bounds on  $\langle\sigma\rangle_{95}^{\text{obs}}$  in each signal region to constrain the parameter space of the fat-brane realization of mUED. We have closely followed the object reconstruction, event selection, and signal region definitions presented in Ref. [2] to obtain bounds on the  $R^{-1}$ - $M_D$  plane for different values of  $N$ . The ATLAS multi-jet search in Ref. [2] has already been implemented and validated in a previous work in Ref. [18] in the context of obtaining bounds on minimal and non-minimal UED models. For brevity, we omit the technical details of the search in Ref. [2]. Interested readers are referred to Ref. [18] for more information.

### 3.4.3 ATLAS di-Photon plus missing transverse energy search [3]

Final state topology with two photons, many soft jets/leptons, and a large missing transverse momentum are common in models with general gauge mediation when the pair-produced squarks and gluinos decay via the cascade involving other lighter SUSY particles to the neutralino NLSP, which in turn, decay into a gravitino LSP in association with a photon. Our fat-brane mUED scenario mimics the above final state topology when the KKNC decays of level-1 KK particles dominate the GMD decay modes. Several analyses at the LHC [3, 101–104] have looked into the diphoton final state in the case of GGM-type models. The most recent ATLAS search for the diphoton plus missing transverse energy final states in Ref. [3] has already been recast in the context of the fat-brane realization

of mUED in Ref. [18], leading to a lower bound on  $R^{-1}$  of 2900 (2700) GeV for  $N = 6(4)$  and  $M_D = 15$  TeV. Note that the ATLAS diphoton search in Ref. [3] corresponds to only  $36.1 \text{ fb}^{-1}$  integrated luminosity data of the 13 TeV LHC. In this work, we have used the diphoton search results in Ref. [3] with a twofold motivation:

1. To reproduce the bounds on  $R^{-1}$  in Ref. [18] and validate our implementation of gravity-mediated decays of level-1 KK particles in PYTHIA8.
2. To extrapolate the results in Ref. [3] to obtain the reach at  $139 \text{ fb}^{-1}$  integrated luminosity of the LHC. Note that the mono-photon and multi-jet searches discussed in the previous paragraphs correspond to  $139 \text{ fb}^{-1}$  of data. Extrapolation of the diphoton search will make the diphoton search comparable to the mono-photon and multi-jet search bounds.

The details of the object selection and signal region definition can be found in [3, 18]; we omit them here for brevity. However, for the sake of completeness of this article, we have presented the definitions of the signal regions used for the ATLAS diphoton analysis of Ref. [3] in Table 4. Table 4 also shows the 95 % CL bound on the visible cross-section in different signal regions that has been obtained by the ATLAS collaboration with  $36.1 \text{ fb}^{-1}$  integrated luminosity data at the 13 TeV LHC. In the last row of Table 4, we have presented the 95 % CL expected upper limits on the visible cross-section in different signal regions with  $139 \text{ fb}^{-1}$  integrated luminosity of the LHC. To obtain the expected limits in the last row in Table 4, we extracted the background cross-section from the expected number of background events provided in Ref. [3] at  $36.1 \text{ fb}^{-1}$  data for the different signal regions. Then, following Refs. [122–124], we use the following approximated expressions for the median expected exclusion significance to estimate the expected upper bound on the signal cross-section at  $139 \text{ fb}^{-1}$  integrated luminosity:

$$Z_{\text{exc}} = \left[ 2 \left\{ s - b \ln \left( \frac{b + s + x}{2b} \right) - \frac{b^2}{\delta_b^2} \ln \left( \frac{b - s + x}{2b} \right) \right\} - (b + s - x)(1 + b/\delta_b^2) \right]^{1/2},$$

where  $x = \sqrt{(s + b)^2 - 4sb\delta_b^2/(b + \delta_b^2)}$ ,  $s$  and  $b$  are the number of signal and background events, respectively, and  $\delta_b$  is the uncertainty in the measurement of the background. For our analysis, we adopt a conservative approach and assume an overall 40% (statistical + systematic) uncertainty in the measurement of the backgrounds. In the absence of any diphoton analysis with the full LHC run II data, we derived the expected reach of the di-photon channel on the  $R^{-1}$ - $M_D$  mass plane.

### 3.4.4 Event Simulation

To generate events for the pair/associated production of level-1 KK quarks/gluons in the framework of the fat-brane realization of the mUED scenario, we used the mUED model file [77, 78, 125] provided in the Feynrules model database. The production of colored level-1 KK particles is simulated in MG5\_AMC@NLO [111] with the NNPDF21LO[126] parton distribution function (PDF). The subsequent decay, showering, and hadronization

Cuts	$SR_{S-L}^{\gamma\gamma}$	$SR_{S-H}^{\gamma\gamma}$
Number of photons	$\geq 2$	$\geq 2$
$p_T(\gamma_1) > [\text{GeV}]$	75	75
$p_T(\gamma_2) > [\text{GeV}]$	75	75
$\cancel{E}_T > [\text{GeV}]$	150	250
$H_T > [\text{TeV}]$	2.75	2.00
$\Delta\phi(\text{jet}, \cancel{E}_T) >$	0.5	0.5
$\Delta\phi(\gamma, \cancel{E}_T) >$	-	0.5
$\langle \epsilon\sigma \rangle_{\text{obs}}^{95} [\text{fb}] (\mathcal{L} = 36.1 \text{ fb}^{-1})$ [3]	0.083	0.083
$\langle \epsilon\sigma \rangle_{\text{exp}}^{95} [\text{fb}] (\mathcal{L} = 139 \text{ fb}^{-1})$	0.0305	0.0305

**Table 4:** Signal regions and cuts used by the ATLAS Collaboration [3] in di-photon search along with the observed 95% C.L. upper limit on model-independent visible beyond the SM cross-section. Here,  $H_T$  is the scalar sum of the transverse energy of photons, any additional jets, and leptons in an event.  $\Delta\phi(\text{jet}, \cancel{E}_T)$  is the azimuthal separation between two leading jets with  $p_T > 75$  GeV and  $\cancel{E}_T$  vector. The other symbols carry their usual meaning.

are simulated in Pythia8 [112]. PYTHIA8 does not consider gravity-mediated decay for the KK particles. Moreover, these decays cannot be trivially incorporated by modifying the decay table of the KK particles in the SLHA file since gravity-mediated decays need to be simulated not to a single gravity excitation but to a member of the tower of gravity excitations. We have incorporated the gravity-mediated decay for the KK particles in PYTHIA8 by modifying the PYTHIA PYWIDTH subroutine according to our requirements. We used the fast detector simulator Delphes to simulate different physics objects like jets, leptons, and photons. For the mono-photon analysis, we have followed the object reconstruction criteria described in 3.4.1. Similarly, for the di-photon and multi-jet analysis, we have followed the prescription for object reconstruction as described in [18, 47] respectively. To generate the bounds on the model parameter space for the mono-photon and multi-jet analysis, we have compared the signal cross-section in the different signal regions with the respective 95 % confidence level upper limits provided by the ATLAS collaboration in Ref. [1] and [2], respectively. On the other hand, for the di-photon analysis, we have reinterpreted the expected number of background events for 139  $\text{fb}^{-1}$  LHC and used it to calculate the 95 % C.L upper limit on the model parameter space. In the next section, we will discuss the bounds on the model parameter space from the different collider analyses.

### 3.4.5 Results

For convenience, we have presented the collider bounds on the parameter space of fat brane realization of mUED for three distinct values of the number of large extra dimensions, denoted as  $N = 2$ ,  $N = 4$ , and  $N = 6$ . Once the value of  $N$  is fixed, the phenomenology of the model is governed by three independent parameters: the cut-off scale  $\Lambda$ , the radius of

compactification for the small extra dimensions  $R$ , and the fundamental Planck mass  $M_D$ . Throughout our analysis, we have fixed  $\Lambda R$  at 5. We have varied  $R^{-1}$  within the 2 to 3.5 TeV range and the fundamental Planck mass  $M_D$  within the 5 to 15 TeV range. We present our results in Figure 5 as bounds on the  $R^{-1}Vs.M_D$  plane. The bounds on the  $R^{-1} - M_D$  plane presented in Figure 5 for  $N = 2$  (top left panel),  $N = 4$  (top right panel), and  $N = 6$  (bottom panel) are discussed in the following.

- Bounds for  $N = 2$  (top left panel):** For the  $N = 2$  scenario, the spacing between the individual gravity excitations is minimum, resulting in a higher density of graviton states compared to cases where  $N$  equals 4 and 6. Consequently, the level-1 KK particles have the freedom to decay into numerous graviton states, leading to a substantial GMD width (see top left panel of Figure 2). At the LHC, the pair produced level-1 quarks/gluons dominantly decay via gravity-mediated processes and result in a final state characterized by high  $p_T$  jets and a significant missing transverse energy. This makes the multi-jet +  $E_T^{miss}$  search the most sensitive for  $N = 2$  and effectively excludes a large part of the parameter space. For instance, it sets a lower limit on  $R^{-1}$  of around 2975 GeV independent of the value of  $M_D$ . The mono-photon analysis, though not as effective as the multi-jet one, excludes  $R^{-1} < 2534(2596)$  GeV for  $M_D = 5(15)$  TeV. The Di-photon analysis, on the other hand, excludes a tiny portion of the  $R^{-1} - M_D$  plane in the upper left corner where KKNC decays start becoming significant (see Figure 2 top left panel).
- Bounds for  $N = 4$  (top right panel):** In this case, the GMD and KKNC decay widths have almost comparable strength (see upper right panel of Figure 2). The former decay mode prevails in the small  $M_D$  region, leading to a final state characterized by multiple jets and a large  $E_T^{miss}$  at the collider. Conversely, the KKNC decays dominate for larger values of  $M_D$ ; hence, mono-photon and diphoton searches can effectively constrain this part of the parameter space. As depicted in 5 (top right panel), the multi-jet search excludes  $R^{-1} < 2898(2800)$  GeV for  $M_D = 5(15)$  TeV. For higher values of  $M_D$ , though the KKNC decays dominate, the final state  $Z$  bosons, followed by its hadronic decay, can contribute to the multi-jet final state. Ergo, we see a comparable performance of the multi-jet SR throughout the range of  $M_D$ . The Mono-Photon analysis is most effective in the upper  $M_D$  region and excludes  $R^{-1} < 2958$  GeV corresponding to  $M_D = 15$  TeV. The di-photon analysis also has comparable performance, and it sets a lower limit of 2874 GeV on  $R^{-1}$  for  $M_D = 15$  TeV.
- Bounds for  $N = 6$  (bottom panel):** For a fixed value of  $M_D$ , as we increase  $N$ , the density of graviton states decreases, resulting in a reduced GMD decay width. Therefore, for the  $N=6$  case, the KKNC decays dominate over the GMD decays for most parts of the parameter space. In this scenario, the specific decay mode of the level-1 photon determines the resulting final state topology. If both  $\gamma^1$  decay via the photon channel, it results in a di-photon final state. If one  $\gamma^1$  follows the photon channel, we get the monophoton final state. Conversely, we get a multijet final state if both  $\gamma^1$  decay to  $Z$ -boson followed by the hadronic decay of both the  $Z$ -boson. For

smaller values of  $M_D$ , the strength of GMD decays increases, resulting in a multijet final state topology at the LHC. In the bottom panel of Figure 5, we summarise our results for the N=6 scenario. The multi-jet signal region excludes  $R^{-1} < 2871(2761)$  GeV for  $M_D = 5(15)$  TeV. The monophoton signal region sets a lower limit of  $R^{-1} = 2599(2886)$  GeV for  $M_D = 5(15)$  TeV. The diphoton search is sensitive in the large  $M_D$  region and leads to an expected reach of  $R^{-1}$  up to 3000 GeV for  $M_D = 15$  TeV at the LHC with  $139 \text{ fb}^{-1}$  integrated luminosity.

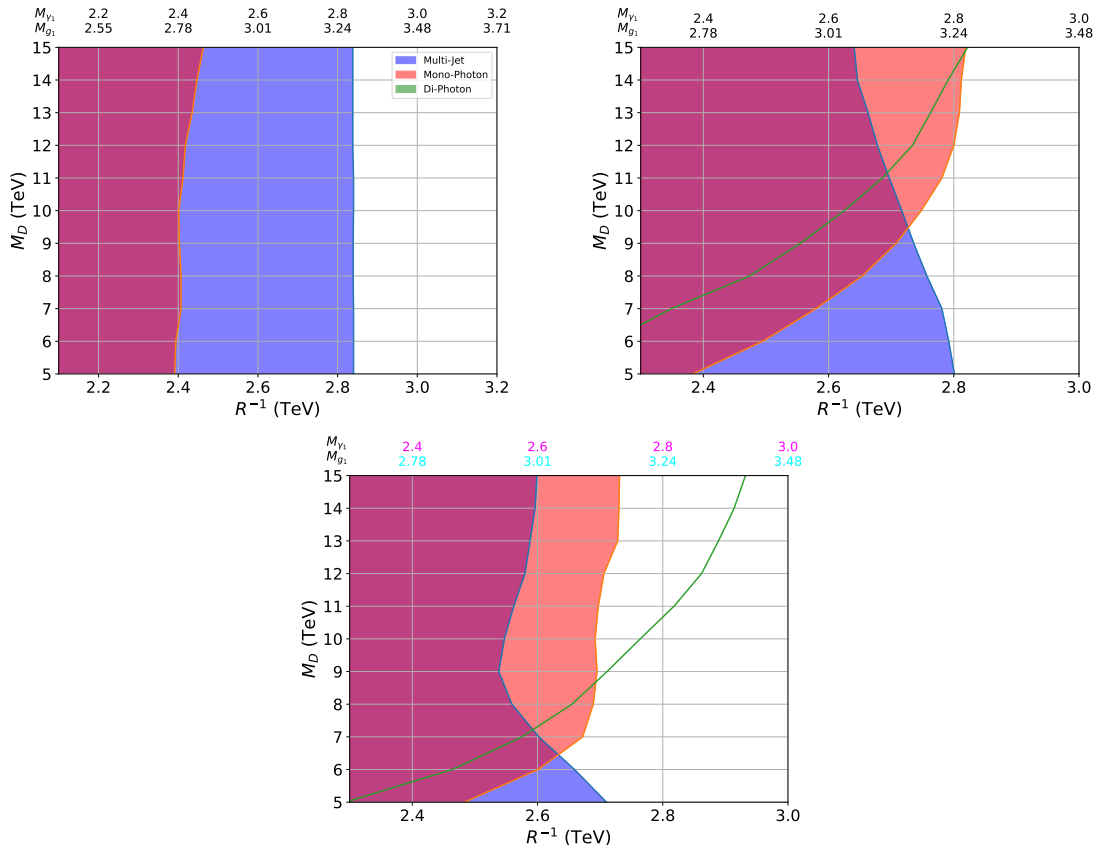


**Figure 5:** The exclusion limits for fat-brane MUED parameter space in the  $R^{-1}$  Vs  $M_D$  plane from the three ATLAS analysis [1–3]. Throughout this paper, we have fixed  $\Lambda R = 5$ . The three plots correspond to N=2(top left), N=4(top right), and N=6(bottom). The limits in the mono-photon and multijet cases are derived from the 95 % C.L. upper limit on the visible cross-section  $\langle \epsilon \sigma \rangle_{obs}^{95}$ . For the Di-Photon signal region, we present the expected  $2\sigma$  C.L. lower limit on the model parameters for  $139 \text{ fb}^{-1}$  luminosity of data collected at the 13 TeV LHC.

### 3.5 Optimized search strategies for the Future LHC Runs

The updated LHC bounds presented in Figure 5 indicate that masses of the level-1 KK-gluon (the heaviest level-1 particle) and level-1 KK photon below approximately 3 TeV have already been excluded, based on the consistency of LHC data with the Standard Model

background predictions. These LHC bounds are derived using the ATLAS mono-photon, diphoton, and multijets search results, which are optimized for various supersymmetric scenarios. For instance, the mono-photon and diphoton searches are designed to target GGM models, while the multijet analysis focuses on detecting squarks and gluons in the R-parity conserving MSSM model. Although the final state topologies from these scenarios resemble those arising from the production and decay of level-1 KK quarks and gluons in the fat-brane realization of the mUED model, the kinematics of the final state particles differ significantly. For example, in the GGM scenario, the photon resulting from the decay of a massive lightest neutralino (ranging from a few hundred GeV to a few TeV) into a nearly massless gravitino is always very energetic. In contrast, in the fat brane mUED scenario, the level-1 KK photon can decay into any KK member of the graviton tower with a mass below that of the level-1 KK photon. Consequently, the energy of the photon from this decay depends on the mass of the KK graviton. A very energetic photon results when the level-1 KK photon decays into a light KK graviton, whereas a decay into a heavier KK graviton results in a softer photon. Therefore, search strategies optimized for SUSY scenarios might not be efficient for the fat brane mUED scenario. The remainder of this article focuses on developing optimized mono-photon, diphoton, and multijet search strategies specifically for the fat brane mUED scenario.

### 3.5.1 Event Generation and Object Reconstruction

For generating the signal events, we have followed the strategy outlined in Section 3.4.4. The model parameter space studied follows the discussion in Section 3.4.5. We have fixed the value of  $\Lambda R$  at five and considered three possible values of the number of large extra dimensions:  $N = 2, 4,$  and  $6$ . For generating the signal events, we have varied  $R^{-1}$  in the range of 2.7 TeV to 3.5 TeV, and for each value of  $R^{-1}$ , we have varied  $M_D$  in the range of 5 to 15 TeV. To present our numerical results (cross-section, kinematic distributions, etc.), we defined three benchmark points in Table 5.

Process	Cross Section (fb)	k-factor	$M_D$ (TeV)
$N = 2$	0.15	1	5
$N = 4$			15
$N = 6$			15

**Table 5:** List of benchmark signal scenarios corresponding to  $R^{-1} = 3.1$  TeV.

As for the SM backgrounds, we have considered all the SM processes contributing to the mono-photon, di-photon, and multi-jet final states [1–3]. The list of SM processes includes single and multi-top production (with associated vector bosons), mono-boson (with additional partons), di-boson, tri boson, and tetra boson production. All background events are generated with up to two additional partons in MG5\_AMC@NLO [111] with the NNPDF21LO [126] parton distribution function. All background events are generated at

leading order (LO), followed by MLM matching using Pythia8 [112], and we subsequently scale the LO crosssection with the appropriate next-to-leading order (NLO) k-factors [127–138]. For completeness, we have listed all the SM background processes considered in our analysis in Table 6.

Backgrounds for the photonic SRs		Backgrounds for the multi-jet SRs	
Process	k-factor	Process	k-factor
$\gamma + jets$	1.66 (Fig.4 of [139])	$t\bar{t} + jets$	1.5 [129]
$\gamma\gamma + jets$	1.66 (Fig.1 of [140])	$V + jets$	1.09 [133, 134]
$t\bar{t}\gamma$	1	$t\bar{t}V$	1.66 [130]
$VV\gamma$	1.8 [141]	$tW + jets$	1.27 [132]
$VV\gamma\gamma$	1	$VV + jets$	1.66 [127]
$W(\rightarrow l\nu)\gamma + jets$	1.31 [127]	$VVV$	2.6 [142]
$W(\rightarrow l\nu)\gamma\gamma$	1		
$Z(\rightarrow \nu\nu)\gamma + jets$	1.18 [127]		
$Z(\rightarrow \nu\nu)\gamma\gamma$	1		

**Table 6:** List of the dominant SM backgrounds considered in our final analysis.

With lower bounds on the KK-quark and KK-gluon masses approaching around 3 TeV (see Figure 5), decays of such massive KK-quarks and KK-gluons are expected to produce highly boosted SM heavy bosons or top quarks in the final state. In particular, the decay of level-1 top quarks or electroweak (EW) gauge bosons into graviton excitations could lead to highly boosted SM  $W$  or  $Z$  bosons in the final state. In a collider like the LHC, the hadronic decays of these boosted bosons/top quarks appear as a collimated beam of hadrons, making it convenient to reconstruct them as a single large-radius (fat) jet. Along with their reconstruction, proper identification of these fat jets is also crucial, as similar fat jets can also arise from QCD radiation. Efficiently identifying hadronically decaying boosted SM heavy bosons or top quarks over QCD jets is anticipated to enhance the discrimination of the signal from the SM background. To distinguish the fat jets originating from these bosons from jets originating from QCD-initiated quarks and gluon jets, our analysis implements a simple boosted decision tree (BDT) classifier. The details of the classifier are discussed in Appendix A.3.

To reconstruct final state jets, leptons, etc., we follow the steps outlined in Section 3.4.1 with a slight modification. In addition to the  $R = 0.4$  radius jets, we also reconstruct fat jets with a radius of 1.0. These fat jets pass through a jet pruning algorithm [143, 144] to eliminate the broad QCD emissions. For our analysis, we have used the default pruning setup of Delphes with parameters: a  $z_{cut}$  value of 0.1 and an  $R_{cut}$  value of 0.5. Reconstructed fat jets are required to have a transverse momentum greater than 300 GeV and pseudorapidity  $|\eta| < 2.5$ . These fat jets are then passed through the BDT classifier and are tagged as either a  $V$  (i.e.,  $W/Z$ ) jet or a QCD jet. For further analysis, we retain only the

$V$ -tagged  $R = 1.0$  radius jets (denoted by  $j^{V\text{-tag}}$  throughout the rest of the manuscript). Since our analysis considers both  $R = 0.4$  jets and  $V$ -tagged  $R = 1.0$  radius jets, we need a strategy to avoid the possibility of double-counting jets. To address this, we exclude any  $R = 0.4$  jets from our analysis if they lie within a cone of radius 1.0 from the center of a  $V$ -tagged jet. The resolved  $R = 0.4$  jets are denoted by  $j^{0.4}$  in the remainder of the manuscript.

### 3.5.2 Event Selection

The signal and background samples are selected by designing appropriate signal regions based on the expected multiplicity of the final state photons, leptons, and jets in the signal processes. The idea is to design mutually independent signal regions that can be statistically combined and, at the same time, capture most of the signal events, thereby maintaining high signal selection efficiency. We achieve this by designing five signal regions (SRs): SR\_1p0l, SR\_1pnl, SR\_2p0l, SR\_2pnl, and SR\_0p0l. We present the preselection requirements defining these signal regions in Table 7 and discuss them in the following sections.

- SR\_1p0l and SR\_1pnl Signal Regions:** The SR\_1p0l signal region is designed to capture final states with a single photon, at least two  $R = 0.4$  jets, and no leptons. As shown in Table 7, additional requirements are imposed on the transverse momentum of the photons and jets, as well as the missing transverse momentum. This signal region is suitable for cases where one NLKP  $\gamma_1$  decays into a photon. This can occur in the  $N = 4$  scenario if one of the intermediate particles in the decay cascade follows the GMD mode, breaking the decay chain, or in both the  $N = 4$  and  $N = 6$  scenarios when one of the two NLKPs decays into a  $Z$  boson. The SR\_1pnl signal region has similar requirements on photons and jets but also requires additional leptons. While it captures similar signal scenarios as SR\_1p0l, the presence of leptons in the final state reduces contributions from the SM background.
- SR\_2p0l and SR\_2pnl Signal Regions:** The SR\_2p0l and SR\_2pnl signal regions are designed to capture final states with two photons and at least two jets, along with additional requirements on the missing transverse momentum and the  $p_T$  of the photons and jets. Like the mono-photon signal regions, these two di-photon signal regions differ in terms of lepton multiplicity. In the SR\_2p0l signal region, a lepton veto is imposed, while the SR\_2pnl signal region requires events with at least one lepton. These signal regions are effective for scenarios where the decay of level-1 quarks/gluons follows the KKNC decay cascade and both NLKP  $\gamma_1$  particles decay to photons. In the SR\_2pnl signal region, additional leptons are expected from the decay cascade and are anticipated to be soft, so no further  $p_T$  cuts on leptons are imposed.
- SR\_0p0l Signal Region:** The SR\_0p0l signal region is specifically designed for the  $N = 2$  scenario, where gravity-mediated decays of level-1 KK quarks/gluons dominate over the KKNC decay mode across most of the parameter space. Consequently,



photons from the GMD decay of  $\gamma_1$  or leptons from the KKNC decay cascade are not expected in the final state, so both a photon veto and a lepton veto are imposed. This signal region requires at least three jets, a large missing transverse momentum, and a minimum transverse momentum for the three leading jets (see Table 7).

Cuts	SR_1p0l	SR_1pnl	SR_2p0l	SR_2pnl	SR_0pnl
$N_\gamma$	1	1	2	2	0
$N_l$	0	$\geq 1$	0	$\geq 1$	0
$N_j$	$\geq 2$	$\geq 2$	$\geq 2$	$\geq 2$	$\geq 3$
$p_T(\gamma_1)$ (GeV)	$> 150$	$> 150$	$> 150$	$> 150$	–
$p_T(j1)$ (GeV)	$> 100$	$> 100$	$> 100$	$> 100$	$> 200$
$p_T(j2)$ (GeV)	$> 50$	$> 50$	$> 50$	$> 50$	$> 100$
$p_T(j3)$ (GeV)	–	–	–	–	$> 50$
$E_T^{miss}$ (GeV)	$> 200$	$> 200$	$> 200$	$> 200$	$> 300$

**Table 7:** Pre-selection cuts for the five signal regions implemented in our analysis.

To analyze the signal and background events in each signal region, we construct several kinematic variables that capture the kinematic properties of the signal and background events. These variables are designed to encode the differences in behavior between signal and background events. By carefully designing constraints on these variables, the background contribution in these signal regions can be suppressed while retaining a significant fraction of the signal events. Determining the optimal set of kinematic cuts requires examining the distribution of these variables for both signal and background samples. The goal is to choose kinematic constraints that sufficiently reduce the background contribution while maintaining high signal efficiency. This involves inspecting these variables individually and in various combinations. As the number of variables increases, this process becomes time-consuming and cumbersome. A more systematic and automated approach is achievable with the help of a machine learning-based classifier. For our final analysis, we have developed five BDT-based classifiers, one for each signal region. The kinematic variables constructed for the signal and background events serve as input to these classifiers, and the output, i.e., the BDT score, can be used as the final discriminating variable between signal and background. All these classifiers use the same hyperparameters as the classifier discussed in Appendix A.3.

We list the observables used for training the BDT classifiers in the five signal regions in Appendix A.4. The list of observables includes missing transverse energy ( $E_T^{miss}$ ),  $H_T$ ,  $M_{\text{eff}}$ ,  $E_T^{miss}/\sqrt{H_T}$ ,  $p_T$  and  $\eta$  of  $R = 0.4$  jets,  $V$ -tagged jets, leptons, and photons; the azimuthal angle ( $\Delta\phi$ ) between the missing transverse energy vector and reconstructed jets, leptons, and photons; and more (see Appendix A.4 for the full list of observables). In Figures 6–10, we present the distributions of three of the most important kinematic variables for each

of the signal regions. All these distributions assume an integrated luminosity of  $500 \text{ fb}^{-1}$ . To enhance visibility, the number of signal events in each bin is multiplied by a factor of 100. For each signal region, we only show the distribution of the dominant backgrounds, along with the distributions for a few benchmark signal scenarios. Since the SR\_1p01, SR\_1pn1, SR\_2p01, and SR\_2pn1 regions are most effective for the  $N = 4$  and  $N = 6$  scenarios, we present results for these two scenarios with fixed values of  $R^{-1} = 3.1 \text{ TeV}$  and  $M_D = 15 \text{ TeV}$ . Similarly, for the SR\_0pnj signal region, we present results for the  $N = 2$  scenario with  $R^{-1} = 3.1 \text{ TeV}$  and  $M_D = 5 \text{ TeV}$ . As expected for each signal region, the missing transverse momentum is the most important observable for discriminating signal from the background, as the signal events typically exhibit large missing transverse energy due to the invisible KK gravity excitation in the final state. The effective mass ( $M_{\text{eff}}$ ), defined as the scalar sum of the transverse momentum of all visible final-state particles and the missing transverse momentum, also plays a crucial role in distinguishing signal from background.

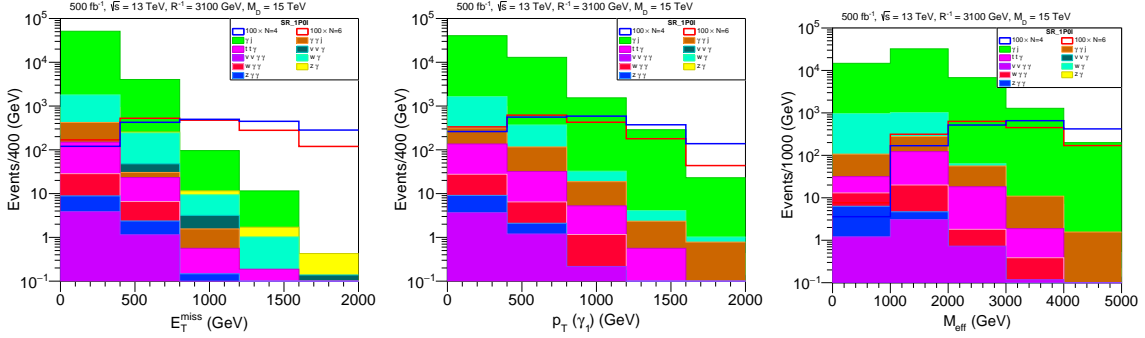


**Figure 6:** Distribution of the top three important kinematic variables for the SR\_1p01 signal region.

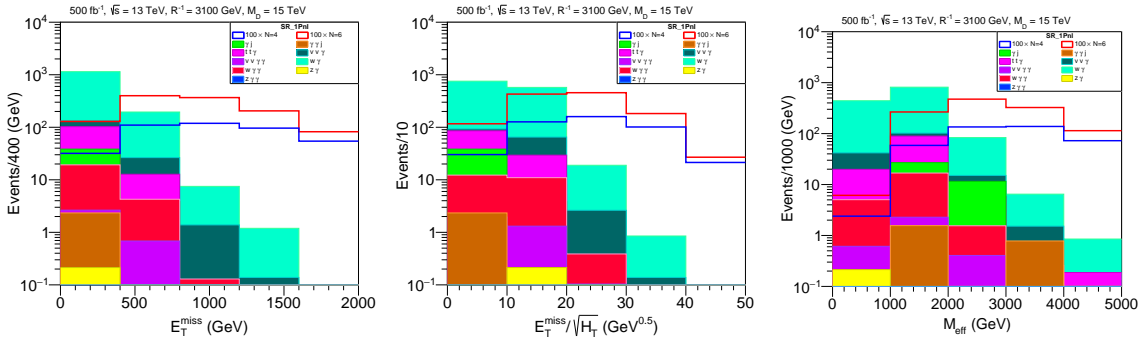


**Figure 7:** Distribution of the top three important kinematic variables for the SR\_1pn1 signal region.

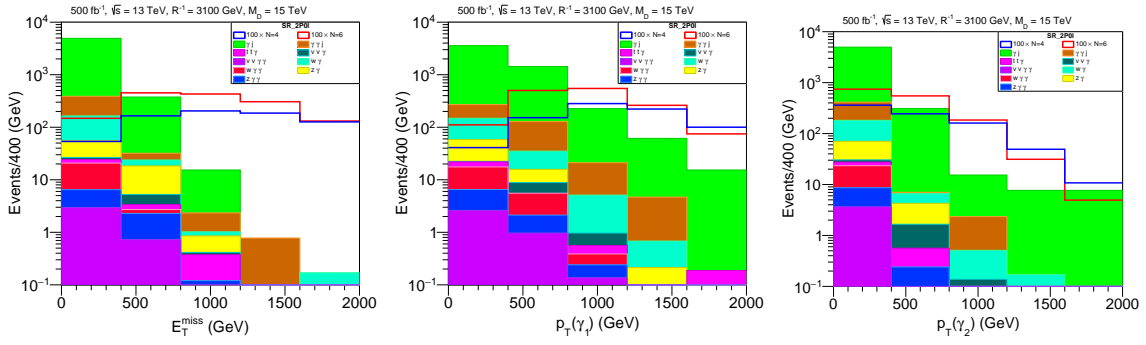


**Figure 8:** Distribution of the top three important kinematic variables for the SR\_2p01 signal region.

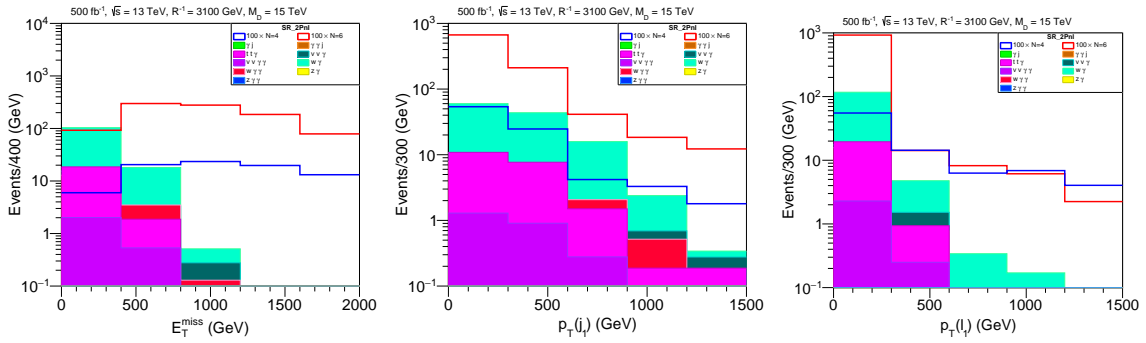


**Figure 9:** Distribution of the top three important kinematic variables for the SR\_2pn1 signal region.

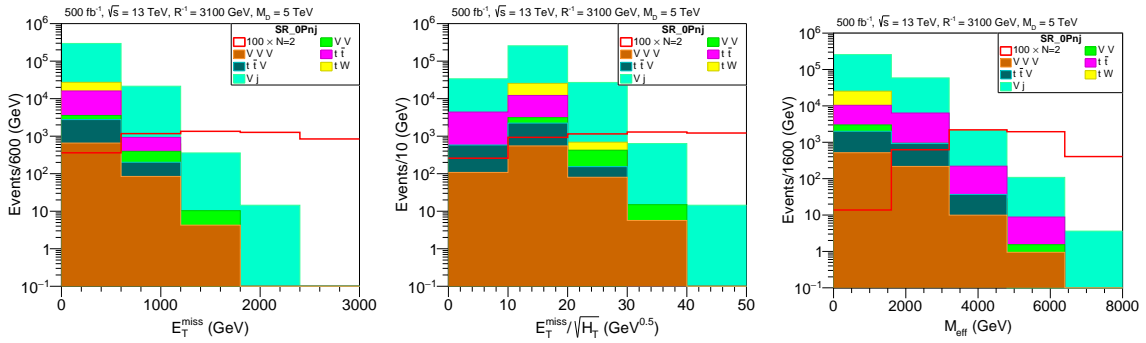


**Figure 10:** Distribution of the top three important kinematic variables for the SR\_0p01 signal region.

### 3.5.3 Results

In this section, we discuss the future projection of the LHC reach on the parameter space of the fat brane MUED scenario. Figure 11 shows the distribution of the signal and background BDT scores from the five classifiers trained on variables constructed from the signal and background events across the five signal regions. Similar to Figures 6–10, for the SR\_1p01, SR\_1pn1, SR\_2p01, and SR\_2pn1 signal regions, we present the BDT score distri-

bution for the  $N = 4$  and  $N = 6$  signal scenarios, with fixed values of  $R^{-1} = 3.1$  TeV and  $M_D = 14$  TeV. For the `SR_0p01` signal region, we show the distribution for the  $N = 2$  signal scenario with  $R^{-1} = 3.1$  TeV and  $M_D = 6$  TeV. The results are presented for a luminosity of  $500 \text{ fb}^{-1}$ . A detailed analysis of the scores suggests that an asymmetric binning of the scores with edges at  $-1, 0, 0.2, 0.4, 0.6,$  and  $1$  provides the most effective separation between signal and background in bins with higher BDT scores. Since the number of background events generated corresponds to the chosen luminosity, the complete absence of background events in the final bin does not present a problem for our analysis.

To determine the signal significance in each signal region, we have statistically combined the number of signal and background events in each bin of the score histogram (see Figure 11) using a profile likelihood approach with the publicly available Python-based package `Spey` [145]. Estimating the background uncertainty in detail is beyond the scope of this work. Thus, we take a conservative approach and assume an overall uncertainty (statistical + systematic) of 20% in the background estimation for our analysis. In Figure 12, we present the required luminosity as a function of  $R^{-1}$  to achieve a median significance of 1.645 (equivalently, 95% C.L.). For convenience, we have fixed  $M_D = 14$  TeV for these plots. Figure 12 provides a quantitative insight into the effectiveness of the signal regions across different signal scenarios. For instance,

- In the  $N = 2$  scenario, the gravity-mediated decay of level-1 KK particles dominates over the KKNC decay modes. As a result, in most events, the produced level-1 quarks and gluons tend to decay directly into gravity excitations, effectively breaking the decay cascade. Consequently, the likelihood of obtaining events with final-state photons—arising from the decay of the level-1 KK photon at the end of the decay chain—is very low. For this reason, the `SR_0pnj` signal region is most effective in constraining the  $N = 2$  scenario.
- In the  $N = 4$  signal scenario, the strength of KKNC decay modes becomes comparable to that of the GMD modes for level-1 EW gauge bosons and leptons. This allows pair-produced KK quarks and gluons to undergo KKNC decays into level-1 EW gauge bosons and leptons. The non-negligible GMD branching ratios for level-1 EW gauge bosons and leptons lead to both mono-photon and di-photon final states. However, due to the reduced SM background contribution, the di-photon final state is expected to provide better sensitivity. This is the behavior we observe in the upper right panel of Figure 12.
- In the  $N = 6$  case, the KKNC decay modes dominate over the GMD modes, making it highly probable that KK particles will follow the complete decay cascade. As a result, most events are expected to produce a final state with two photons. This explains the improved sensitivity observed for the `SR_2p01` and `SR_2pn1` signal regions in the plot shown in the bottom panel of Figure 12.

In Figures 13 and 14, we present the expected significance for different values of  $R^{-1}$  and  $M_D$  for the three scenarios:  $N = 2, 4,$  and  $6$ . Based on the previous discussion, we

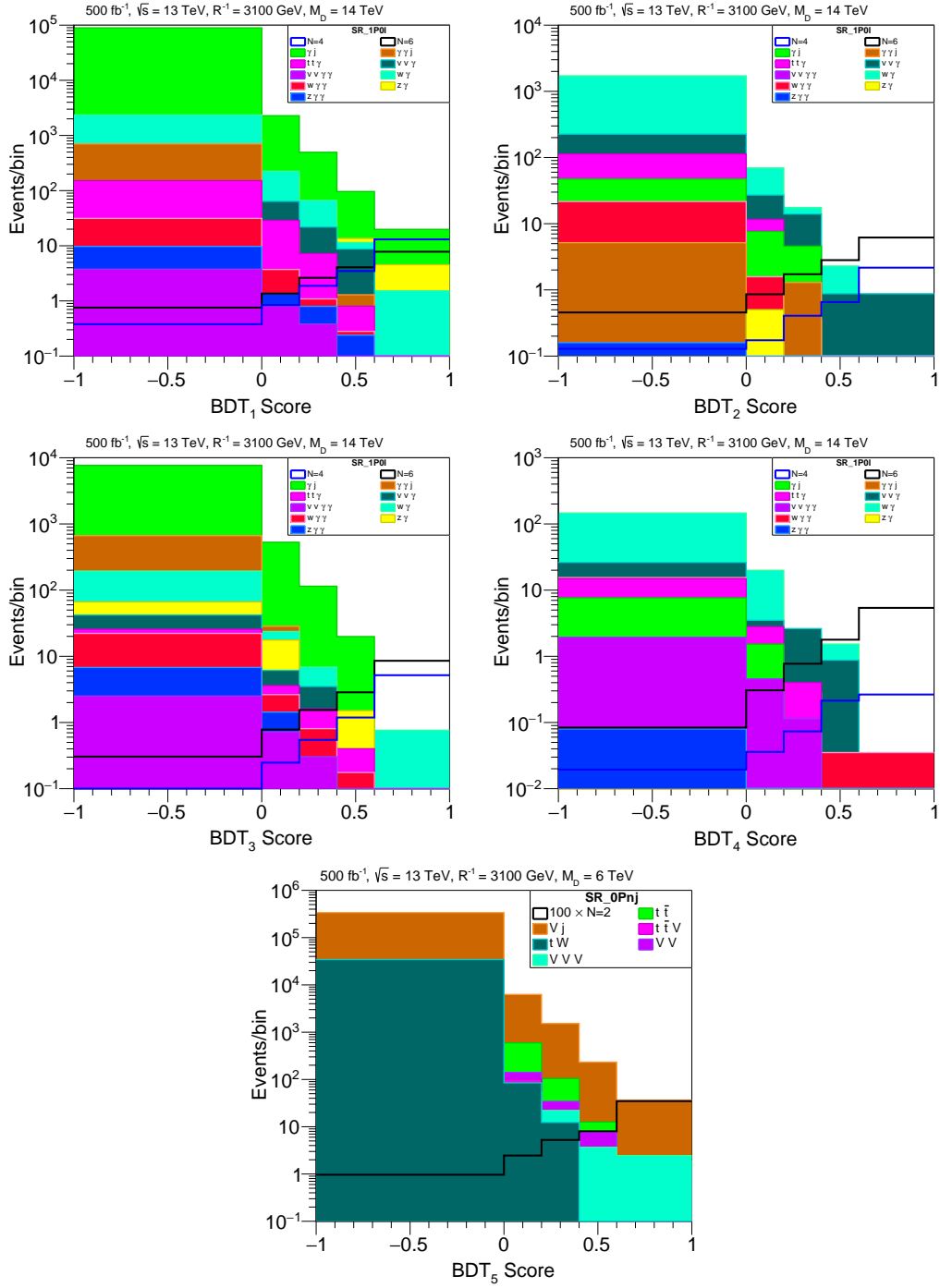


**Figure 11:** Distribution of BDT score for the signal and background events in the five signal regions.

only include results for the key signal regions for each benchmark scenario. All results are computed assuming a luminosity of  $500 \text{ fb}^{-1}$ .

- For the  $N = 2$  signal scenario, only the SR\_0pnj signal region is relevant. The

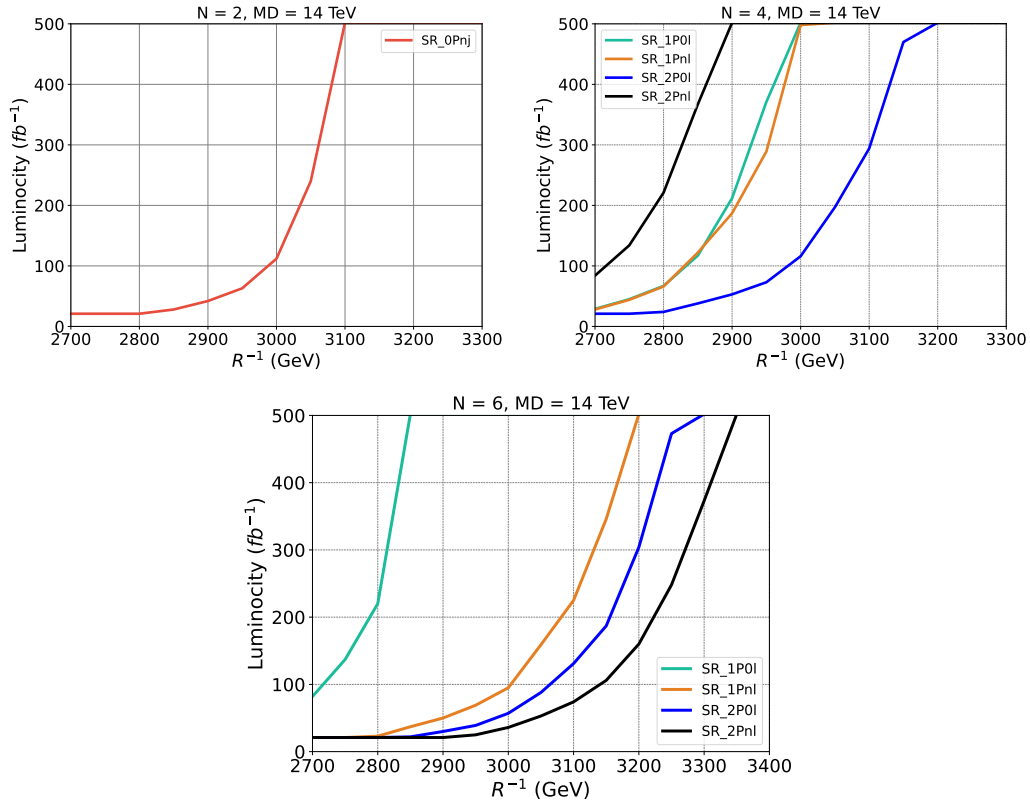


**Figure 12:** Required luminosity as a function of  $R^{-1}$  to achieve a median significance of 1.645 (equivalently, 95% C.L.).

corresponding result is shown in the upper left panel of Figure 13. Note that the significance does not depend on  $M_D$ . The parameter  $M_D$  determines the density of gravity states, where a higher  $M_D$  corresponds to a lower density, reducing the available gravity states for KK particles to decay into and thus reducing the GMD decay width. However, for the  $N = 2$  scenario, the GMD decay consistently dominates over the KKNC decays, as shown in the upper left plot of Figure 13.

- For the  $N = 4$  scenario, we show the reach of the SR\_1pn1 (top right panel of Figure 13), SR\_2p01 (bottom left panel of Figure 13), and SR\_0pnj (bottom right panel of Figure 13) signal regions. In this case, the GMD and KKNC decay widths are comparable, making the effect of  $M_D$  more pronounced. For higher  $M_D$  values, the KKNC decay modes dominate, enhancing the sensitivity of the mono-photon and diphoton regions, as observed in the top right and bottom left panels of Figure 13. For lower  $M_D$  values, the GMD decay width dominates, making the SR\_0pnj region the most efficient. However, the reach of SR\_0pnj is weaker than in the  $N = 2$  case, as the gravity excitation mass spectrum tends to peak at higher values (See Figure 1), producing softer jets that may not meet the signal selection criteria.
- Figure 14 presents our results for the  $N = 6$  scenario in the SR\_1p0l, SR\_1pn1,

SR\_2p01, and SR\_2pn1 signal regions. As discussed, the two di-photon regions show greater sensitivity due to reduced background and the dominance of the KKNC decay mode.

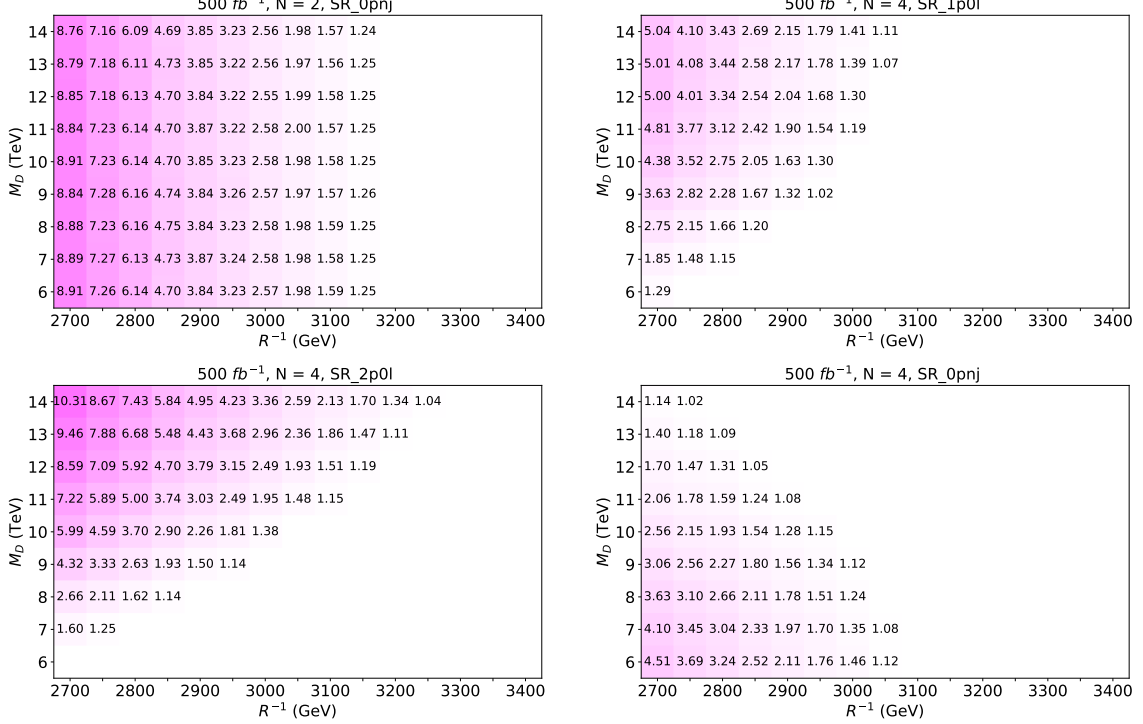


**Figure 13:** Significance for different values of  $R^{-1}$  and  $M_D$  for the  $N = 2$  (upper left) and  $N = 4$  (other three) signal scenarios. We only present the results for the important signal regions (see text) for each case.

In Figure 15, we present the significance achieved by statistically combining the number of signal and background events across each signal region for different values of  $R^{-1}$  and  $M_D$ . The results are based on an integrated luminosity of  $500 \text{ fb}^{-1}$ . The upper left panel of Figure 15 displays the results for the  $N = 2$  scenario, showing that with  $500 \text{ fb}^{-1}$  of luminosity, the LHC can probe  $R^{-1}$  values up to  $3090 \text{ GeV}$  at 95% C.L. significance across the full  $M_D$  range of 6 to 14 TeV. In the  $N = 4$  scenario, shown in the upper right panel of Figure 15, a 95% C.L. sensitivity extends up to  $R^{-1} = 3190 \text{ GeV}$  for an  $M_D$  value around 14 TeV. Similarly, in the  $N = 6$  scenario (bottom panel), sensitivity reaches approximately  $3390 \text{ GeV}$  for an  $M_D$  value near 14 TeV.

## 4 Summary and Outlook

We conducted a comprehensive study on the fat-brane MUED scenario, which involves expanding MUED to include additional dimensions ranging from  $eV^{-1}$  to  $KeV^{-1}$  that can

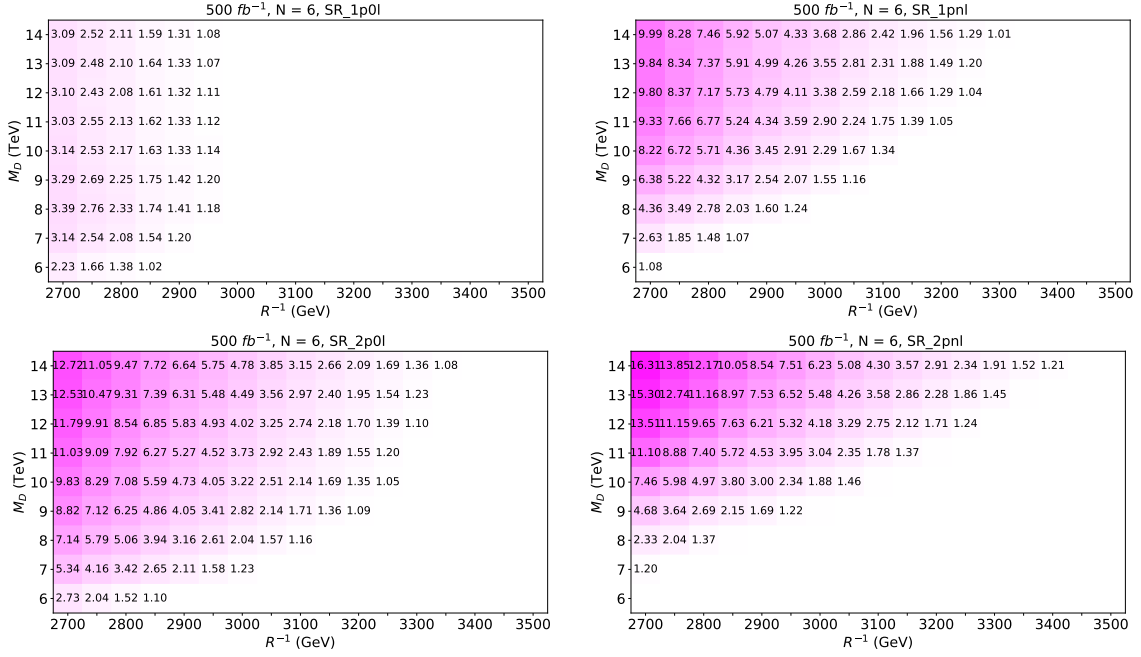


**Figure 14:** Significance for different values of  $R^{-1}$  and  $M_D$  for the  $N = 6$  signal scenario.

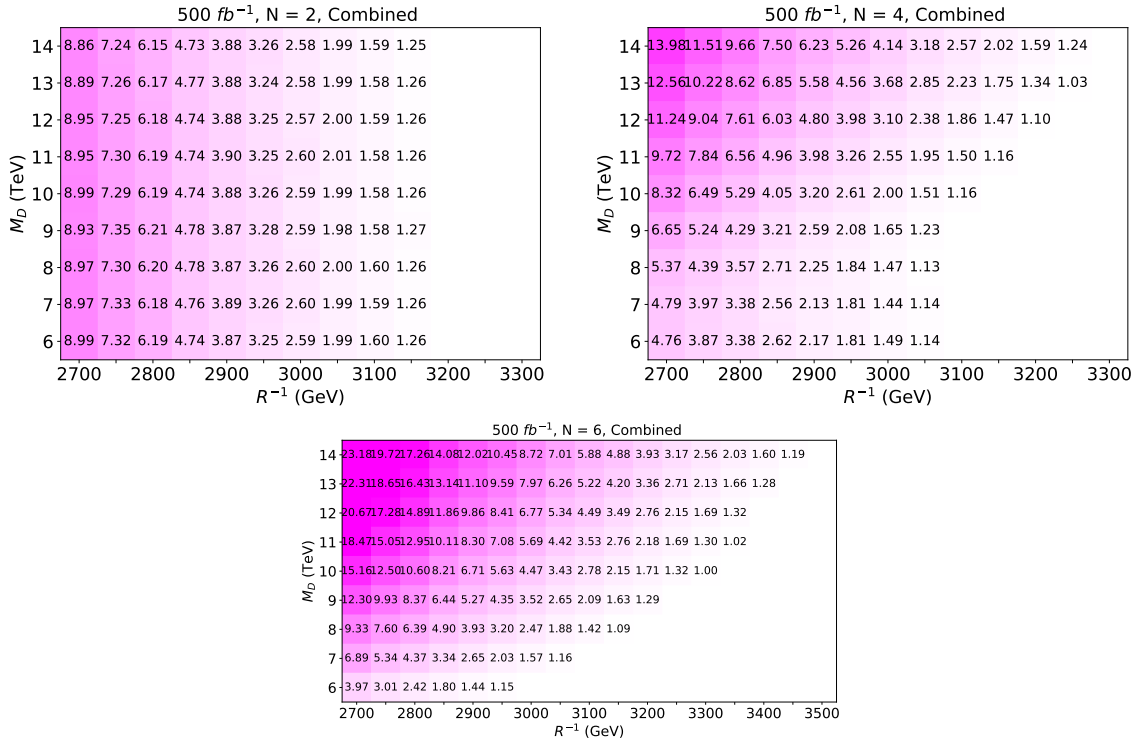


**Figure 15:** Combined significance for different values of  $R^{-1}$  and  $M_D$  for the three signal scenarios:  $N = 2$  (upper left),  $N = 4$  (upper right), and  $N = 6$  (bottom).



only be accessed by gravity. By considering the decay mode of the level-1 photon, we identified three possible final state topologies at the LHC: the multijet, mono-photon, and diphoton final states. LHC has already performed searches for similar final states in the case of the MSSM and Gauge Mediated supersymmetry breaking models. In light of the observations being consistent with the predicted SM backgrounds, model-independent 95% C.L. upper limits have been set on the visible cross-section. In our analysis, we have incorporated three such searches by the ATLAS collaboration, enabling us to impose constraints on the parameter space of the fat-brane MUED model. For the N=2 scenario, the multijet search has the best reach and excludes  $R^{-1}$  below 2975 GeV independent of the value of  $M_D$ . For the N=4 case, the multi-jet and mono-photon searches probe complementary parts of the parameter space. The former(latter) excludes  $R^{-1} < 2898(2958)$  for  $M_D = 500(15000)$  GeV. For the case where N=6, the di-photon search is most effective and sets a lower limit of 3002 GeV on  $R^{-1}$  for  $M_D = 15000$  GeV. The low- $M_D$  region of the parameter space is also sensitive to the multijet search, and for a  $M_D$  of 5000 GeV, it excludes  $R^{-1}$  below 2871 GeV.

Further, we forecast future limits at the 13 TeV LHC for  $500 \text{ fb}^{-1}$  of integrated luminosity by proposing a novel search strategy that yields improved limits on the parameter space on interest. Our strategy advocates the implementation of fat jets and uses two BDT classifiers to discern top and W/Z fat jets from QCD fat jets. We also consider signal regions without fat jets, where we have modified the previous ATLAS analysis to improve their reach. Implementing our strategy, we project a lower limit of around 3320 GeV on  $R^{-1}$  throughout the range of  $M_D$  for the N=2 scenario, which is 345 GeV higher than the previous estimate. For the case where N=4 we can exclude  $R^{-1}$  below 2942(3157) for  $M_D = 5000(15000)$  GeV. As for the N=6 case, our proposed analysis has a reach of up to 3021(3225) GeV in  $R^{-1}$  for  $M_D = 5000(15000)$  GeV.

To conclude this section, it is worth mentioning that the fat jet signal regions hold promising potential for investigating the aforementioned parameter space provided the use of a classifier with superior performance, which we have deferred to future research endeavors.

## ACKNOWLEDGMENTS

KG acknowledges the financial support (MTR/2022/000989) provided by the MATRICS research grant, titled "*Exploring Next-to-Minimal Realizations of Universal Extra-Dimension Scenarios*", funded by the Science and Engineering Research Board (SERB). KG also gratefully acknowledges the local hospitality provided by the Helsinki Institute of Physics, University of Helsinki, during his visit to Helsinki, where a significant portion of this project was conducted. The simulations were partly supported by the SAMKHYA: High-Performance Computing Facility provided by the Institute of Physics, Bhubaneswar.

## A Appendix

### A.1 GMD widths of level-1 KK particles

The gravity mediated decay width of KK-1 fermions is given by [94],

$$\begin{aligned}
\Gamma(q^l \rightarrow qh^{\vec{n}}) &= |F_{l|\vec{n}}^c|^2 \frac{k^2}{2 \times 384\pi} \frac{M^3}{x^4} [(1-x^2)^4(2+3x^2)] \\
\Gamma(q^l \rightarrow qA^{\vec{n}}) &= |F_{l|\vec{n}}^s|^2 \frac{k^2}{2 \times 256\pi} M^3 [(1-x^2)^2(2+x^2)] P_{55} \\
\Gamma(q^l \rightarrow q\phi^{\vec{n}}) &= |F_{l|\vec{n}}^c|^2 \frac{k^2}{2 \times 256\pi} M^3 (1-x^2)^2 [c_{11} \frac{(1-x^2)^2}{x^4} + 2c_{12} \frac{1-x^2}{x^2} + c_{22}]
\end{aligned} \tag{A.1}$$

Where  $M = 1/R$  is the mass of the matter excitation,  $x = m_{\vec{n}}/M$  with  $m_{\vec{n}}$ , the mass of the gravity mode. The form factor  $F_{l|\vec{n}}^{c/s}$  and the coefficients  $P_{55}, c_{ij}$  appear because the gravity excitations are not all independent. They have the following forms:

$$\begin{aligned}
|F_{l|\vec{n}}^c|^2 &= \frac{4}{\pi^2} \frac{x_5^2}{(1-x_5^2)^2} [1 + \cos(\pi x_5)] \\
|F_{l|\vec{n}}^s|^2 &= \frac{|F_{l|\vec{n}}^c|^2}{x_5^2} \\
P_{55} &= 1 - \frac{n_5^2}{n^2} \\
c_{11} &= \omega^2(N-1) \\
c_{12} &= -\frac{2}{N+2} P_{55} \\
c_{22} &= \frac{2(N+1)}{(N+2)} P_{55}^2
\end{aligned} \tag{A.2}$$

where,  $x_5 = 2\pi n_5 R/(lr)$ . We can have similar expressions for the GMD decay width of KK-1 gauge bosons,

$$\begin{aligned}
\Gamma(V^l \rightarrow Vh^{\vec{n}}) &= |F_{l|\vec{n}}^c|^2 \frac{k^2}{3 \times 96\pi} \frac{M^3}{x^4} [(1-x^2)^3(1+3x^2+6x^4)] \\
\Gamma(V^l \rightarrow VA^{\vec{n}}) &= |F_{l|\vec{n}}^s|^2 \frac{k^2}{3 \times 32\pi} \frac{M^3}{x^2} [(1-x^2)^3(1+x^2)] P_{55} \\
\Gamma(V^l \rightarrow V\phi^{\vec{n}}) &= |F_{l|\vec{n}}^c|^2 \frac{k^2}{3 \times 128\pi} M^3 (1-x^2)^3 [c_{11} \frac{1}{x^4} + 2c_{12} \frac{1}{x^2} + c_{22}]
\end{aligned} \tag{A.3}$$

### A.2 Cut-flow chat for SRM and SRH signal regions

In Tables 8 and 9 we present the cut-flow tables for the SRM and SRH signal regions, respectively.

### A.3 BDT classifier

In this section, we will discuss the BDT classifier used in our analysis for boosted boson tagging. To train the classifier, we require both signal and background fat jet samples. To

Cuts	$m_{\tilde{g}} = 2000\text{GeV}, m_{\tilde{\chi}_1^0} = 250\text{GeV}$			
	$\gamma/Z$		$\gamma/h$	
	Hepdata	Our Result	Hepdata	Our Result
Trigger (one photon $p_T > 140$ Gev)	79.60	81.73	71.29	75.56
At least one photon	79.51	81.73	71.24	75.56
Lepton Veto	50.15	52.45	49.02	52.78
Leading photon $p_T > 300$ Gev	42.33	40.26	41.87	40.38
$E_T^{miss} > 300$ Gev	35.55	33.80	35.29	33.74
Number of Jets $\geq 5$	34.52	33.54	34.22	33.5
$\Delta\phi(jet, E_T^{miss}) > 0.4$	29.50	28.68	29.24	28.49
$\Delta\phi(\gamma, E_T^{miss}) > 0.4$	28.43	27.73	28.55	27.65
$H_T > 1600$ GeV	25.86	23.81	26.54	24.65
$R_T^4 < 0.9$	21.81	21.57	22.66	22.25

**Table 8:** Cut-Flow table for the SRM signal region. The entries in the second and fourth columns are the results provided by the Atlas collaboration [1] in the form of Hepdata. The entries in the third and fifth columns represent our simulated results.

Cuts	$m_{\tilde{g}} = 2000\text{GeV}, m_{\tilde{\chi}_1^0} = 250\text{GeV}$			
	$\gamma/Z$		$\gamma/h$	
	Hepdata	Our Result	Hepdata	Our Result
Trigger (one photon $p_T > 140$ Gev)	92.73	92.3	76.03	77.61
At least one photon	92.72	92.3	76.01	77.61
Lepton Veto	88.15	88.79	73.73	74.93
Leading photon $p_T > 400$ Gev	83.18	81.6	69.48	68.39
$E_T^{miss} > 600$ Gev	65.41	64.03	54.66	53.06
Number of Jets $\geq 3$	51.19	58.76	41.12	41.03
$\Delta\phi(jet, E_T^{miss}) > 0.4$	42.84	48.53	35.02	34.66
$\Delta\phi(\gamma, E_T^{miss}) > 0.4$	42.70	48.33	34.92	34.50
$H_T > 1600$ GeV	26.28	27.95	23.60	23.36

**Table 9:** Cut-Flow table for the SRH signal region. The entries in the second and fourth columns are the results provided by the Atlas collaboration [1] in the form of Hepdata. The entries in the third and fifth columns represent our simulated results.

generate the signal fat jets, we have considered the processes  $pp \rightarrow W + W -$  and  $pp \rightarrow ZZ$ , and for the background fat jets, di-jet production is considered. In our analysis, we do not distinguish between the W and Z jets, and we consider them collectively to be V jets.

For training the classifier, we have used the TMVA 4.3 toolkit [146] integrated into ROOT 6.24[147]. The training and evaluation process uses 1.5M fatjets of both V and QCD types. BDT, being a simple cut-based classifier, utilizes high-level features/variables (HLF). Before constructing these variables for our analysis, we pass the signal and background fat jets through a truth-level tagging stage. For signal fat jets, we demand that both the parent boson and all its decay products be present inside the cone of the fat jets. Similarly, for the QCD jets, we demand that the partonic quark/gluon be present inside the reconstruction radius. This truth level tagging enhances the purity of the sample, i.e., it ensures that the signal and background fat jets used for the training/evaluation of the classifier are properly reconstructed. These truth-tagged jets are then split in the ratio of 80:20 for training and testing the classifiers.

To train our classifier, we use the five kinematic features of the fat jets:

**The invariant mass** of the fat jets is reconstructed from the four-momentum of the constituents. It has the following form

$$M = \sqrt{\sum_i (E_i)^2 - \sum_i (p_i)^2} \quad (\text{A.4})$$

where the sum runs over all constituents of the fat jet.

**The Jet Charge** [148] is reconstructed from the charge of individual tracks inside the fat jet, and we define it as,

$$Q_k = \frac{\sum_i q_i (p_{T_i})^k}{\sum_i p_{T_i}} \quad (\text{A.5})$$

Where  $p_{T_i}$  are the transverse momentum associated with the tracks of charge  $q_i$  and  $k$ , the regularisation exponent has a value of 0.2 for our analysis.

**The N-subjettiness variable**  $\tau_N$  [149] gives a quantitative measure of the likeliness of a fat jet to have N substructures. We define it as,

$$\tau_N = \frac{1}{\sum_k p_{T_k} R_0^\beta} \sum_k p_{T_k} \min(\Delta R_{1,k}^\beta \dots \Delta R_{N,k}^\beta) \quad (\text{A.6})$$

where the sum runs over all the jet constituents,  $\beta$  is the thrust parameter,  $R_0$  is the radius of the reconstruction cone, and  $\Delta R_{i,k}$  characterize the separation between the constituent  $k$  and the candidate sub jet  $i$ .

**b-tag** is a boolean observable that takes a value of 1 when at least one of the sub-jets inside a fat jet is a b-jet.

Table 10 summarizes the BDT hyperparameters used while training the classifiers. In Table 11, we present the method-unspecific and method-specific ranking of the kinematical variables used for training our classifiers. The table on the top corresponds to the top vs. QCD case, while that on the bottom corresponds to the W/Z vs. QCD classifier. Finally, we present the covariance matrix for the input features in Figure 16.

BDT hyperparameter	Optimised choice
NTrees	1000
MinNodeSize	5%
MaxDepth	4
BoostType	AdaBoost
AdaBoostBeta	0.1
UseBaggedBoost	True
BaggedSampleFraction	0.5
SeparationType	GiniIndex
nCuts	-1

**Table 10:** Summary of optimised BDT hyperparameters.

Feature	Method-unspecific separation	Method-specific ranking
$m$	0.0427	0.49
$\tau_{21}$	0.387	0.326
$\tau_{32}$	0.055	0.112
$Q_k$	0.012	0.031
$b$ -tag	0.019	0.03

**Table 11:** Method-unspecific separation and method-specific ranking of the input features.

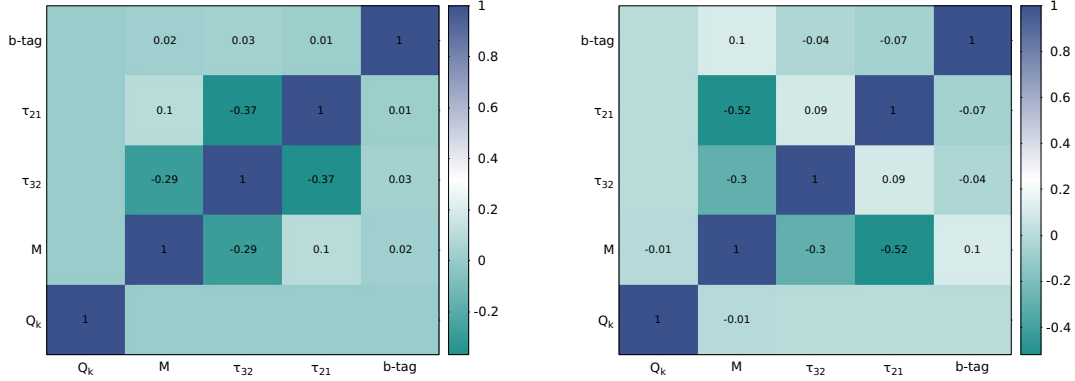


**Figure 16:** Correlations among the input features for the W/Z jets (left) and the QCD jets (right).

We evaluate the performance of the classifier in terms of its receiver-operator-characteristic (ROC) curves and present our result in Fig. 17. The ROC curve also serves as a valuable tool in aiding the selection of the threshold BDT score for our final analysis. We find a threshold of 0.34, which corresponds to a signal efficiency of 60%, suitable for our analysis.

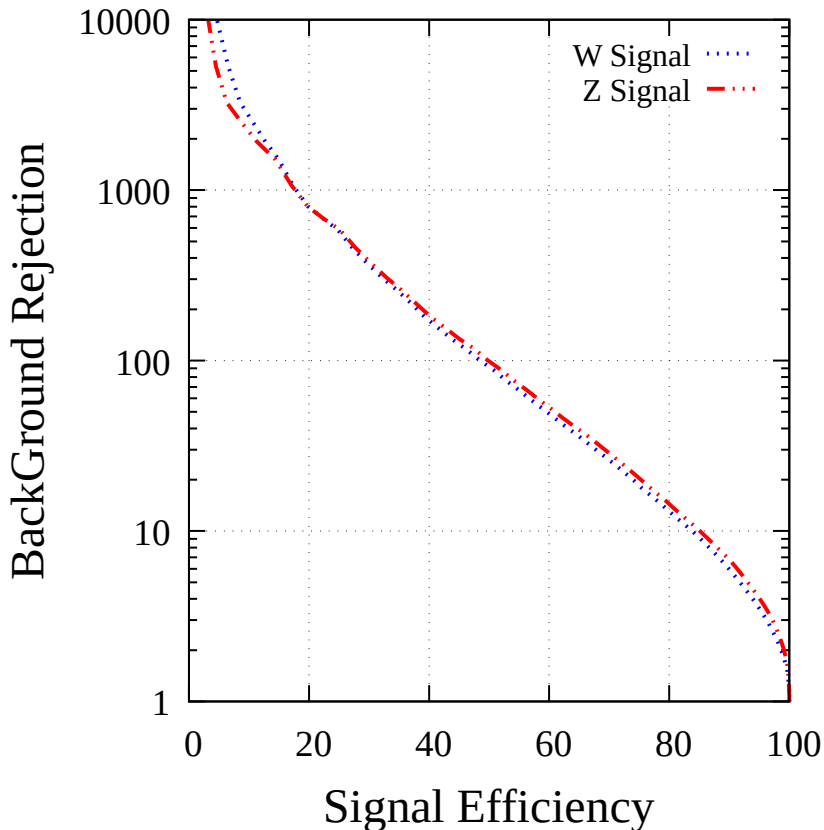


**Figure 17:** The ROC curves for the W/Z vs. QCD classifier. We have defined background rejection as the reciprocal of background efficiency.

#### A.4 Variables constructed for the different signal regions

In Table 12, we present the list of variables constructed from events in the five signal regions and used in the training and evaluation of the BDT classifier. Only variables with checkmarks are used during the analysis. Most of these variables are self-explanatory.  $\Delta\phi(i, j)$  stands for the separation between the particles  $i$  and  $j$  in the azimuthal plane. The azimuthal separation of different final state objects with the missing transverse momentum can help reduce background where a major contribution to the missing energy comes from objects that are not properly identified/reconstructed. The azimuthal separation between photons and leptons is expected to be higher for backgrounds like  $W\gamma$  and  $W\gamma\gamma$  where the lepton from the  $W$  boson and the photon are more likely to get produced back to back. The variables  $H_T$ , defined as the scalar sum of the transverse momentum of all visible final state particles,  $M_{eff} = (H_T + E_T^{miss})$ , missing transverse momentum significance ( $E_T^{miss}/\sqrt{H_T}$ ) are expected to have a higher value for the signal events considering the high mass of the level-1 KK particles involved. In Table 12, we have denoted with  $j$  and  $j^{1.0}$  final state jets with reconstruction radius 0.4 and 1.0, respectively, while the numbers in the subscript denote their  $p_T$  ordering. For events with no fat jets or less than three  $R = 0.4$  jets, the corresponding transverse momentum variables and azimuthal separation with missing

transverse momentum are zero-padded.

Variable	SR_1p0l	SR_1pnl	SR_2p0l	SR_2pnl	SR_0pnj
$E_T^{miss}$	✓	✓	✓	✓	✓
$p_T(j_1)$	✓	✓	✓	✓	✓
$p_T(j_2)$	✓	✓	✓	✓	✓
$p_T(j_3)$	✓	✓	×	×	✓
$p_T(\gamma_1)$	✓	✓	✓	✓	×
$p_T(\gamma_2)$	×	×	✓	✓	×
$p_T(l_1)$	×	✓	×	✓	×
$p_T(j_1^{1,0})$	✓	✓	✓	✓	✓
$\Delta\phi(j_1, E_T^{miss})$	✓	✓	✓	✓	✓
$\Delta\phi(j_2, E_T^{miss})$	✓	✓	✓	✓	✓
$\Delta\phi(j_3, E_T^{miss})$	✓	✓	×	×	✓
$\Delta\phi(\gamma_1, E_T^{miss})$	✓	✓	✓	✓	×
$\Delta\phi(\gamma_2, E_T^{miss})$	×	×	✓	✓	×
$\Delta\phi(\gamma_1, l_1)$	×	✓	×	✓	×
$\Delta\phi(\gamma_2, l_1)$	×	×	×	✓	×
$\eta(j_1)$	×	×	×	×	✓
$\eta(j_2)$	×	×	×	×	✓
$H_T$	✓	✓	✓	✓	✓
$E_T^{miss}/\sqrt{H_T}$	✓	✓	✓	✓	✓
$M_{eff}$	✓	✓	✓	✓	✓
$N(j \neq b)$	✓	✓	✓	✓	✓
$N(j = b)$	✓	✓	✓	✓	✓
$N(j^{1,0})$	✓	✓	✓	✓	✓
$N(l)$	×	✓	×	✓	×
$N(\gamma)$	×	×	✓	✓	×

**Table 12:** Variables used for the training of BDT classifiers.

## References

- [1] **ATLAS** Collaboration, *Search for new phenomena in final states with photons, jets and missing transverse momentum in pp collisions at  $\sqrt{s} = 13$  TeV with the ATLAS detector*, [arXiv:2206.06012](#).
- [2] **ATLAS** Collaboration, *Search for squarks and gluinos in final states with jets and missing transverse momentum using  $139 \text{ fb}^{-1}$  of  $\sqrt{s} = 13$  TeV pp collision data with the ATLAS detector*, *ATLAS-CONF-2019-040*, 8, 2019.
- [3] **ATLAS** Collaboration, M. Aaboud et al., *Search for photonic signatures of gauge-mediated supersymmetry in 13 TeV pp collisions with the ATLAS detector*, *Phys. Rev. D* **97** (2018), no. 9 092006, [[arXiv:1802.03158](#)].

- [4] N. Arkani-Hamed, S. Dimopoulos, and G. R. Dvali, *The Hierarchy problem and new dimensions at a millimeter*, *Phys. Lett. B* **429** (1998) 263–272, [[hep-ph/9803315](#)].
- [5] I. Antoniadis, *A Possible new dimension at a few TeV*, *Phys. Lett. B* **246** (1990) 377–384.
- [6] I. Antoniadis, N. Arkani-Hamed, S. Dimopoulos, and G. R. Dvali, *New dimensions at a millimeter to a Fermi and superstrings at a TeV*, *Phys. Lett. B* **436** (1998) 257–263, [[hep-ph/9804398](#)].
- [7] L. Randall and R. Sundrum, *A Large mass hierarchy from a small extra dimension*, *Phys. Rev. Lett.* **83** (1999) 3370–3373, [[hep-ph/9905221](#)].
- [8] L. Randall and R. Sundrum, *An Alternative to compactification*, *Phys. Rev. Lett.* **83** (1999) 4690–4693, [[hep-th/9906064](#)].
- [9] T. Appelquist, H.-C. Cheng, and B. A. Dobrescu, *Bounds on universal extra dimensions*, *Phys. Rev. D* **64** (2001) 035002, [[hep-ph/0012100](#)].
- [10] G. Servant and T. M. P. Tait, *Is the lightest Kaluza-Klein particle a viable dark matter candidate?*, *Nucl. Phys. B* **650** (2003) 391–419, [[hep-ph/0206071](#)].
- [11] K. Kong and K. T. Matchev, *Precise calculation of the relic density of Kaluza-Klein dark matter in universal extra dimensions*, *JHEP* **01** (2006) 038, [[hep-ph/0509119](#)].
- [12] B. A. Dobrescu, D. Hooper, K. Kong, and R. Mahbubani, *Spinless photon dark matter from two universal extra dimensions*, *JCAP* **10** (2007) 012, [[arXiv:0706.3409](#)].
- [13] B. A. Dobrescu and E. Poppitz, *Number of fermion generations derived from anomaly cancellation*, *Phys. Rev. Lett.* **87** (2001) 031801, [[hep-ph/0102010](#)].
- [14] T. Appelquist, B. A. Dobrescu, E. Ponton, and H.-U. Yee, *Proton stability in six-dimensions*, *Phys. Rev. Lett.* **87** (2001) 181802, [[hep-ph/0107056](#)].
- [15] A. Belyaev, M. Brown, J. Moreno, and C. Papineau, *Discovering Minimal Universal Extra Dimensions (MUED) at the LHC*, *JHEP* **06** (2013) 080, [[arXiv:1212.4858](#)].
- [16] T. Kakuda, K. Nishiwaki, K.-y. Oda, and R. Watanabe, *Universal extra dimensions after Higgs discovery*, *Phys. Rev. D* **88** (2013) 035007, [[arXiv:1305.1686](#)].
- [17] G. Belanger, A. Belyaev, M. Brown, M. Kakizaki, and A. Pukhov, *Testing Minimal Universal Extra Dimensions Using Higgs Boson Searches at the LHC*, *Phys. Rev. D* **87** (2013), no. 1 016008, [[arXiv:1207.0798](#)].
- [18] K. Ghosh, D. Karabacak, and S. Nandi, *Universal Extra Dimension models with gravity mediated decays after LHC Run II data*, *Phys. Lett. B* **788** (2019) 388–395, [[arXiv:1805.11124](#)].
- [19] K. Ghosh and A. Datta, *Probing two Universal Extra Dimensions at International Linear Collider*, *Phys. Lett. B* **665** (2008) 369–373, [[arXiv:0802.2162](#)].
- [20] K. Ghosh and A. Datta, *Phenomenology of spinless adjoints in two Universal Extra Dimensions*, *Nucl. Phys. B* **800** (2008) 109–126, [[arXiv:0801.0943](#)].
- [21] J. Beuria, A. Datta, D. Debnath, and K. T. Matchev, *LHC Collider Phenomenology of Minimal Universal Extra Dimensions*, *Comput. Phys. Commun.* **226** (2018) 187–205, [[arXiv:1702.00413](#)].
- [22] U. K. Dey and A. Raychaudhuri, *KK-number non-conserving decays: Signal of  $n = 2$  excitations of extra-dimensional models at the LHC*, *Nucl. Phys. B* **893** (2015) 408–419, [[arXiv:1410.1463](#)].



- [23] L. Edelhuser, T. Flacke, and M. Kramer, *Constraints on models with universal extra dimensions from dilepton searches at the LHC*, *JHEP* **08** (2013) 091, [[arXiv:1302.6076](#)].
- [24] T. Flacke, A. Menon, and Z. Sullivan, *Constraints on UED from  $W'$  searches*, *Phys. Rev. D* **86** (2012) 093006, [[arXiv:1207.4472](#)].
- [25] G.-Y. Huang, K. Kong, and S. C. Park, *Bounds on the Fermion-Bulk Masses in Models with Universal Extra Dimensions*, *JHEP* **06** (2012) 099, [[arXiv:1204.0522](#)].
- [26] T. Flacke and C. Pasold, *Constraints on split-UED from Electroweak Precision Tests*, *Phys. Rev. D* **85** (2012) 126007, [[arXiv:1111.7250](#)].
- [27] K. Nishiwaki, K.-y. Oda, N. Okuda, and R. Watanabe, *Heavy Higgs at Tevatron and LHC in Universal Extra Dimension Models*, *Phys. Rev. D* **85** (2012) 035026, [[arXiv:1108.1765](#)].
- [28] H. Murayama, M. M. Nojiri, and K. Tobioka, *Improved discovery of a nearly degenerate model: MUED using  $MT2$  at the LHC*, *Phys. Rev. D* **84** (2011) 094015, [[arXiv:1107.3369](#)].
- [29] D. Choudhury, A. Datta, D. K. Ghosh, and K. Ghosh, *Exploring two Universal Extra Dimensions at the CERN LHC*, *JHEP* **04** (2012) 057, [[arXiv:1109.1400](#)].
- [30] K. Ghosh, S. Mukhopadhyay, and B. Mukhopadhyaya, *Discrimination of low missing energy look-alikes at the LHC*, *JHEP* **10** (2010) 096, [[arXiv:1007.4012](#)].
- [31] B. Bhattacharjee and K. Ghosh, *Search for the minimal universal extra dimension model at the LHC with  $\sqrt{s}=7$  TeV*, *Phys. Rev. D* **83** (2011) 034003, [[arXiv:1006.3043](#)].
- [32] G. Bertone, K. Kong, R. Ruiz de Austri, and R. Trotta, *Global fits of the Minimal Universal Extra Dimensions scenario*, *Phys. Rev. D* **83** (2011) 036008, [[arXiv:1010.2023](#)].
- [33] A. Freitas and K. Kong, *Two universal extra dimensions and spinless photons at the ILC*, *JHEP* **02** (2008) 068, [[arXiv:0711.4124](#)].
- [34] C. Macesanu, C. D. McMullen, and S. Nandi, *Collider implications of universal extra dimensions*, *Phys. Rev. D* **66** (2002) 015009, [[hep-ph/0201300](#)].
- [35] K. Ghosh and K. Huitu, *Constraints on Universal Extra Dimension models with gravity mediated decays from ATLAS diphoton search*, *JHEP* **06** (2012) 042, [[arXiv:1203.1551](#)].
- [36] D. Choudhury, A. Datta, and K. Ghosh, *Deciphering Universal Extra Dimension from the top quark signals at the CERN LHC*, *JHEP* **08** (2010) 051, [[arXiv:0911.4064](#)].
- [37] T. G. Rizzo, *Probes of universal extra dimensions at colliders*, *Phys. Rev. D* **64** (2001) 095010, [[hep-ph/0106336](#)].
- [38] A. Muck, A. Pilaftsis, and R. Ruckl, *Probing minimal 5-D extensions of the standard model: From LEP to an  $e^+e^-$  linear collider*, *Nucl. Phys. B* **687** (2004) 55–75, [[hep-ph/0312186](#)].
- [39] G. Bhattacharyya, P. Dey, A. Kundu, and A. Raychaudhuri, *Probing universal extra dimension at the international linear collider*, *Phys. Lett. B* **628** (2005) 141–147, [[hep-ph/0502031](#)].
- [40] M. Battaglia, A. Datta, A. De Roeck, K. Kong, and K. T. Matchev, *Contrasting supersymmetry and universal extra dimensions at the clic multi-TeV  $e^+e^-$  collider*, *JHEP* **07** (2005) 033, [[hep-ph/0502041](#)].
- [41] B. Bhattacharjee and A. Kundu, *The International linear collider as a Kaluza-Klein factory*, *Phys. Lett. B* **627** (2005) 137–144, [[hep-ph/0508170](#)].

- [42] A. Datta, K. Kong, and K. T. Matchev, *Discrimination of supersymmetry and universal extra dimensions at hadron colliders*, *Phys. Rev. D* **72** (2005) 096006, [[hep-ph/0509246](#)]. [Erratum: *Phys.Rev.D* 72, 119901 (2005)].
- [43] A. Datta, G. L. Kane, and M. Toharia, *Is it SUSY?*, [hep-ph/0510204](#).
- [44] CMS Collaboration, V. Khachatryan et al., *Search for dark matter, extra dimensions, and unparticles in monojet events in proton–proton collisions at  $\sqrt{s} = 8$  TeV*, *Eur. Phys. J. C* **75** (2015), no. 5 235, [[arXiv:1408.3583](#)].
- [45] A. Datta, U. K. Dey, A. Raychaudhuri, and A. Shaw, *Boundary Localized Terms in Universal Extra-Dimensional Models through a Dark Matter perspective*, *Phys. Rev. D* **88** (2013) 016011, [[arXiv:1305.4507](#)].
- [46] T. Flacke, D. W. Kang, K. Kong, G. Mohlabeng, and S. C. Park, *Electroweak Kaluza-Klein Dark Matter*, *JHEP* **04** (2017) 041, [[arXiv:1702.02949](#)].
- [47] Avnish, K. Ghosh, T. Jha, and S. Niyogi, *Minimal and non-minimal Universal Extra Dimension models in the light of LHC data at 13 TeV*, *Phys. Rev. D* **103** (2021) 115011, [[arXiv:2012.15137](#)].
- [48] T. Flacke, A. Menon, and D. J. Phalen, *Non-minimal universal extra dimensions*, *Phys. Rev. D* **79** (2009) 056009, [[arXiv:0811.1598](#)].
- [49] A. Datta, K. Nishiwaki, and S. Niyogi, *Non-minimal Universal Extra Dimensions: The Strongly Interacting Sector at the Large Hadron Collider*, *JHEP* **11** (2012) 154, [[arXiv:1206.3987](#)].
- [50] T. Flacke, K. Kong, and S. C. Park, *126 GeV Higgs in Next-to-Minimal Universal Extra Dimensions*, *Phys. Lett. B* **728** (2014) 262–267, [[arXiv:1309.7077](#)].
- [51] A. Datta, K. Nishiwaki, and S. Niyogi, *Non-minimal Universal Extra Dimensions with Brane Local Terms: The Top Quark Sector*, *JHEP* **01** (2014) 104, [[arXiv:1310.6994](#)].
- [52] T. Flacke, K. Kong, and S. C. Park, *Phenomenology of Universal Extra Dimensions with Bulk-Masses and Brane-Localized Terms*, *JHEP* **05** (2013) 111, [[arXiv:1303.0872](#)].
- [53] A. Shaw, *Status of exclusion limits of the KK-parity non-conserving resonance production with updated 13 TeV LHC*, *Acta Phys. Polon. B* **49** (2018) 1421, [[arXiv:1709.08077](#)].
- [54] A. De Rujula, A. Donini, M. B. Gavela, and S. Rigolin, *Fat brane phenomena*, *Phys. Lett. B* **482** (2000) 195–204, [[hep-ph/0001335](#)].
- [55] A. Donini and S. Rigolin, *Anisotropic type I string compactification, winding modes and large extra dimensions*, *Nucl. Phys. B* **550** (1999) 59–76, [[hep-ph/9901443](#)].
- [56] I. Antoniadis, K. Benakli, and M. Quiros, *Direct collider signatures of large extra dimensions*, *Phys. Lett. B* **460** (1999) 176–183, [[hep-ph/9905311](#)].
- [57] D. A. Dicus, C. D. McMullen, and S. Nandi, *Collider implications of Kaluza-Klein excitations of the gluons*, *Phys. Rev. D* **65** (2002) 076007, [[hep-ph/0012259](#)].
- [58] C. Macesanu, C. D. McMullen, and S. Nandi, *New Signal for Universal Extra Dimensions*, *Phys. Lett. B* **546** (2002) 253–260, [[hep-ph/0207269](#)].
- [59] C. Macesanu, S. Nandi, and C. M. Rujoiu, *Monojet and single photon signals from universal extra dimensions*, *Phys. Rev. D* **73** (2006) 076001, [[hep-ph/0510350](#)].
- [60] C. Macesanu, S. Nandi, and M. Rujoiu, *Single Kaluza Klein production in universal extra dimensions*, *Phys. Rev. D* **71** (2005) 036003, [[hep-ph/0407253](#)].

- [61] E. Gabrielli and B. Mele, *Gravitational decays of heavy particles in large extra dimensions*, *Nucl. Phys. B* **647** (2002) 319–343, [[hep-ph/0205099](#)].
- [62] C. Macesanu, A. Mitov, and S. Nandi, *Gravity and matter in extra dimensions*, *Phys. Rev. D* **68** (2003) 084008, [[hep-ph/0305029](#)].
- [63] B. A. Dobrescu, D. Hooper, K. Kong, and R. Mahbubani, *Spinless photon dark matter from two universal extra dimensions*, *Journal of Cosmology and Astroparticle Physics* **2007** (oct, 2007) 012.
- [64] M. T. Arun, D. Choudhury, and D. Sachdeva, *Living Orthogonally: Quasi-universal Extra Dimensions*, *JHEP* **01** (2019) 230, [[arXiv:1805.01642](#)].
- [65] H.-C. Cheng, J. L. Feng, and K. T. Matchev, *Kaluza-Klein dark matter*, *Phys. Rev. Lett.* **89** (2002) 211301, [[hep-ph/0207125](#)].
- [66] D. Hooper and S. Profumo, *Dark Matter and Collider Phenomenology of Universal Extra Dimensions*, *Phys. Rept.* **453** (2007) 29–115, [[hep-ph/0701197](#)].
- [67] M. Colom i Bernadich and C. Pérez de los Heros, *Limits on Kaluza–Klein dark matter annihilation in the Sun from recent IceCube results*, *Eur. Phys. J. C* **80** (2020), no. 2 129, [[arXiv:1912.04585](#)].
- [68] M. Kakizaki, S. Matsumoto, and M. Senami, *Relic abundance of dark matter in the minimal universal extra dimension model*, *Phys. Rev. D* **74** (2006) 023504, [[hep-ph/0605280](#)].
- [69] F. Burnell and G. D. Kribs, *The Abundance of Kaluza-Klein dark matter with coannihilation*, *Phys. Rev. D* **73** (2006) 015001, [[hep-ph/0509118](#)].
- [70] Y. Ishigure, M. Kakizaki, and A. Santa, *Thermal relic abundance of the lightest Kaluza-Klein particle in phenomenological universal extra dimension models*, [[arXiv:1611.06760](#)].
- [71] J. M. Cornell, S. Profumo, and W. Shepherd, *Dark matter in minimal universal extra dimensions with a stable vacuum and the “right” Higgs boson*, *Phys. Rev. D* **89** (2014), no. 5 056005, [[arXiv:1401.7050](#)].
- [72] K. Kong, S. C. Park, and T. G. Rizzo, *A vector-like fourth generation with a discrete symmetry from Split-UED*, *JHEP* **07** (2010) 059, [[arXiv:1004.4635](#)].
- [73] C.-R. Chen, M. M. Nojiri, S. C. Park, J. Shu, and M. Takeuchi, *Dark matter and collider phenomenology of split-UED*, *JHEP* **09** (2009) 078, [[arXiv:0903.1971](#)].
- [74] S. C. Park and J. Shu, *Split Universal Extra Dimensions and Dark Matter*, *Phys. Rev. D* **79** (2009) 091702, [[arXiv:0901.0720](#)].
- [75] F. del Aguila, M. Perez-Victoria, and J. Santiago, *Bulk fields with general brane kinetic terms*, *JHEP* **02** (2003) 051, [[hep-th/0302023](#)].
- [76] M. Carena, T. M. P. Tait, and C. E. M. Wagner, *Branes and Orbifolds are Opaque*, *Acta Phys. Polon. B* **33** (2002) 2355, [[hep-ph/0207056](#)].
- [77] H.-C. Cheng, K. T. Matchev, and M. Schmaltz, *Radiative corrections to Kaluza-Klein masses*, *Phys. Rev. D* **66** (2002) 036005, [[hep-ph/0204342](#)].
- [78] H.-C. Cheng, K. T. Matchev, and M. Schmaltz, *Bosonic supersymmetry? Getting fooled at the CERN LHC*, *Phys. Rev. D* **66** (2002) 056006, [[hep-ph/0205314](#)].

- [79] **WMAP** Collaboration, E. Komatsu et al., *Seven-Year Wilkinson Microwave Anisotropy Probe (WMAP) Observations: Cosmological Interpretation*, *Astrophys. J. Suppl.* **192** (2011) 18, [[arXiv:1001.4538](#)].
- [80] **Planck** Collaboration, P. A. R. Ade et al., *Planck 2015 results. XIII. Cosmological parameters*, *Astron. Astrophys.* **594** (2016) A13, [[arXiv:1502.01589](#)].
- [81] M. Dine, W. Fischler, and M. Srednicki, *Supersymmetric Technicolor*, *Nucl. Phys. B* **189** (1981) 575–593.
- [82] S. Dimopoulos and S. Raby, *Supercolor*, *Nucl. Phys. B* **192** (1981) 353–368.
- [83] M. Dine and W. Fischler, *A Phenomenological Model of Particle Physics Based on Supersymmetry*, *Phys. Lett. B* **110** (1982) 227–231.
- [84] C. R. Nappi and B. A. Ovrut, *Supersymmetric Extension of the  $SU(3) \times SU(2) \times U(1)$  Model*, *Phys. Lett. B* **113** (1982) 175–179.
- [85] L. Alvarez-Gaume, M. Claudson, and M. B. Wise, *Low-Energy Supersymmetry*, *Nucl. Phys. B* **207** (1982) 96.
- [86] S. Dimopoulos and S. Raby, *Geometric Hierarchy*, *Nucl. Phys. B* **219** (1983) 479.
- [87] M. Dine and A. E. Nelson, *Dynamical supersymmetry breaking at low-energies*, *Phys. Rev. D* **48** (1993) 1277–1287, [[hep-ph/9303230](#)].
- [88] M. Dine, A. E. Nelson, and Y. Shirman, *Low-energy dynamical supersymmetry breaking simplified*, *Phys. Rev. D* **51** (1995) 1362–1370, [[hep-ph/9408384](#)].
- [89] M. Dine, A. E. Nelson, Y. Nir, and Y. Shirman, *New tools for low-energy dynamical supersymmetry breaking*, *Phys. Rev. D* **53** (1996) 2658–2669, [[hep-ph/9507378](#)].
- [90] G. F. Giudice and R. Rattazzi, *Theories with gauge mediated supersymmetry breaking*, *Phys. Rept.* **322** (1999) 419–499, [[hep-ph/9801271](#)].
- [91] A. Datta, A. Datta, and S. Poddar, *Enriching the exploration of the  $mUED$  model with event shape variables at the CERN LHC*, *Phys. Lett. B* **712** (2012) 219–225, [[arXiv:1111.2912](#)].
- [92] K. Kong, K. Matchev, and G. Servant, *Extra Dimensions at the LHC*, pp. 306–324, 1, 2010. [[arXiv:1001.4801](#)].
- [93] P. Bandyopadhyay, B. Bhattacharjee, and A. Datta, *Search for Higgs bosons of the Universal Extra Dimensions at the Large Hadron Collider*, *JHEP* **03** (2010) 048, [[arXiv:0909.3108](#)].
- [94] C. MACESANU, *The phenomenology of universal extra dimensions at hadron colliders*, *International Journal of Modern Physics A* **21** (apr, 2006) 2259–2296.
- [95] T. Han, J. D. Lykken, and R.-J. Zhang, *Kaluza-klein states from large extra dimensions*, *Phys. Rev. D* **59** (Mar, 1999) 105006.
- [96] G. F. Giudice, R. Rattazzi, and J. D. Wells, *Quantum gravity and extra dimensions at high-energy colliders*, *Nuclear Physics B* **544** (apr, 1999) 3–38.
- [97] C. Macesanu, A. Mitov, and S. Nandi, *Gravity and matter in extra dimensions*, *Phys. Rev. D* **68** (Oct, 2003) 084008.
- [98] A. Datta and S. Raychaudhuri, *Vacuum Stability Constraints and LHC Searches for a*

- Model with a Universal Extra Dimension*, *Phys. Rev. D* **87** (2013), no. 3 035018, [[arXiv:1207.0476](#)].
- [99] A. Datta, A. Patra, and S. Raychaudhuri, *Higgs Boson Decay Constraints on a Model with a Universal Extra Dimension*, *Phys. Rev. D* **89** (2014), no. 9 093008, [[arXiv:1311.0926](#)].
- [100] K. Ghosh and K. Huitu, *Constraints on universal extra dimension models with gravity mediated decays from ATLAS diphoton search*, *Journal of High Energy Physics* **2012** (jun, 2012).
- [101] **ATLAS** Collaboration, M. Aaboud et al., *Search for supersymmetry in a final state containing two photons and missing transverse momentum in  $\sqrt{s} = 13$  TeV pp collisions at the LHC using the ATLAS detector*, *Eur. Phys. J. C* **76** (2016), no. 9 517, [[arXiv:1606.09150](#)].
- [102] **CMS** Collaboration, A. M. Sirunyan et al., *Search for supersymmetry in events with at least one photon, missing transverse momentum, and large transverse event activity in proton-proton collisions at  $\sqrt{s} = 13$  TeV*, *JHEP* **12** (2017) 142, [[arXiv:1707.06193](#)].
- [103] **CMS** Collaboration, A. M. Sirunyan et al., *Search for gauge-mediated supersymmetry in events with at least one photon and missing transverse momentum in pp collisions at  $\sqrt{s} = 13$  TeV*, *Phys. Lett. B* **780** (2018) 118–143, [[arXiv:1711.08008](#)].
- [104] **ATLAS** Collaboration, G. Aad et al., *Search for photonic signatures of gauge-mediated supersymmetry in 8 TeV pp collisions with the ATLAS detector*, *Phys. Rev. D* **92** (2015), no. 7 072001, [[arXiv:1507.05493](#)].
- [105] M. Cacciari, G. P. Salam, and G. Soyez, *The anti- $k_t$  jet clustering algorithm*, *JHEP* **04** (2008) 063, [[arXiv:0802.1189](#)].
- [106] M. Cacciari, G. P. Salam, and G. Soyez, *FastJet User Manual*, *Eur. Phys. J. C* **72** (2012) 1896, [[arXiv:1111.6097](#)].
- [107] **CMS** Collaboration, S. Chatrchyan et al., *Search for excited leptons in pp collisions at  $\sqrt{s} = 7$  TeV*, *Phys. Lett. B* **720** (2013) 309–329, [[arXiv:1210.2422](#)].
- [108] J. Haase, *Study of the electron  $\rightarrow$  photon misidentification rate in the ATLAS detector*, Master’s thesis, Hamburg U., 2011.
- [109] F. Staub, *SARAH 4 : A tool for (not only SUSY) model builders*, *Comput. Phys. Commun.* **185** (2014) 1773–1790, [[arXiv:1309.7223](#)].
- [110] W. Porod and F. Staub, *SPheno 3.1: Extensions including flavour, CP-phases and models beyond the MSSM*, *Comput. Phys. Commun.* **183** (2012) 2458–2469, [[arXiv:1104.1573](#)].
- [111] J. Alwall, R. Frederix, S. Frixione, V. Hirschi, F. Maltoni, O. Mattelaer, H. S. Shao, T. Stelzer, P. Torrielli, and M. Zaro, *The automated computation of tree-level and next-to-leading order differential cross sections, and their matching to parton shower simulations*, *JHEP* **07** (2014) 079, [[arXiv:1405.0301](#)].
- [112] C. Bierlich et al., *A comprehensive guide to the physics and usage of PYTHIA 8.3*, [[arXiv:2203.11601](#)].
- [113] S. Ambrosanio, G. L. Kane, G. D. Kribs, S. P. Martin, and S. Mrenna, *Search for supersymmetry with a light gravitino at the Fermilab Tevatron and CERN LEP colliders*, *Phys. Rev. D* **54** (1996) 5395–5411, [[hep-ph/9605398](#)].

- [114] J. Dutta, P. Konar, S. Mondal, B. Mukhopadhyaya, and S. K. Rai, *Search for a compressed supersymmetric spectrum with a light Gravitino*, *JHEP* **09** (2017) 026, [[arXiv:1704.04617](#)].
- [115] **DELPHES 3** Collaboration, J. de Favereau, C. Delaere, P. Demin, A. Giammanco, V. Lemaître, A. Mertens, and M. Selvaggi, *DELPHES 3, A modular framework for fast simulation of a generic collider experiment*, *JHEP* **02** (2014) 057, [[arXiv:1307.6346](#)].
- [116] **CMS** Collaboration, V. Khachatryan et al., *A search for new phenomena in pp collisions at  $\sqrt{s} = 13$  TeV in final states with missing transverse momentum and at least one jet using the  $\alpha_T$  variable*, *Eur. Phys. J. C* **77** (2017), no. 5 294, [[arXiv:1611.00338](#)].
- [117] **CMS** Collaboration, V. Khachatryan et al., *Search for new physics with the  $M_{T2}$  variable in all-jets final states produced in pp collisions at  $\sqrt{s} = 13$  TeV*, *JHEP* **10** (2016) 006, [[arXiv:1603.04053](#)].
- [118] **CMS** Collaboration, V. Khachatryan et al., *Inclusive search for supersymmetry using razor variables in pp collisions at  $\sqrt{s} = 13$  TeV*, *Phys. Rev. D* **95** (2017), no. 1 012003, [[arXiv:1609.07658](#)].
- [119] **CMS** Collaboration, A. M. Sirunyan et al., *Search for supersymmetry in multijet events with missing transverse momentum in proton-proton collisions at 13 TeV*, *Phys. Rev. D* **96** (2017), no. 3 032003, [[arXiv:1704.07781](#)].
- [120] **CMS** Collaboration, A. M. Sirunyan et al., *Search for new phenomena with the  $M_{T2}$  variable in the all-hadronic final state produced in proton-proton collisions at  $\sqrt{s} = 13$  TeV*, *Eur. Phys. J. C* **77** (2017), no. 10 710, [[arXiv:1705.04650](#)].
- [121] **CMS** Collaboration, A. M. Sirunyan et al., *Search for natural and split supersymmetry in proton-proton collisions at  $\sqrt{s} = 13$  TeV in final states with jets and missing transverse momentum*, *JHEP* **05** (2018) 025, [[arXiv:1802.02110](#)].
- [122] G. Cowan, K. Cranmer, E. Gross, and O. Vitells, *Asymptotic formulae for likelihood-based tests of new physics*, *Eur. Phys. J. C* **71** (2011) 1554, [[arXiv:1007.1727](#)]. [Erratum: *Eur.Phys.J.C* 73, 2501 (2013)].
- [123] T. P. Li and Y. Q. Ma, *Analysis methods for results in gamma-ray astronomy*, *Astrophys. J.* **272** (1983) 317–324.
- [124] R. D. Cousins, J. T. Linnemann, and J. Tucker, *Evaluation of three methods for calculating statistical significance when incorporating a systematic uncertainty into a test of the background-only hypothesis for a Poisson process*, *Nucl. Instrum. Meth. A* **595** (2008), no. 2 480–501, [[physics/0702156](#)].
- [125] A. Datta, K. Kong, and K. T. Matchev, *Minimal Universal Extra Dimensions in CalcHEP/CompHEP*, *New J. Phys.* **12** (2010) 075017, [[arXiv:1002.4624](#)].
- [126] **NNPDF** Collaboration, R. D. Ball et al., *Parton distributions for the LHC Run II*, *JHEP* **04** (2015) 040, [[arXiv:1410.8849](#)].
- [127] J. M. Campbell, R. K. Ellis, and C. Williams, *Vector boson pair production at the LHC*, *JHEP* **07** (2011) 018, [[arXiv:1105.0020](#)].
- [128] Y.-B. Shen, R.-Y. Zhang, W.-G. Ma, X.-Z. Li, and L. Guo, *NLO QCD and electroweak corrections to WWW production at the LHC*, *Phys. Rev. D* **95** (2017), no. 7 073005, [[arXiv:1605.00554](#)].
- [129] C. Muselli, M. Bonvini, S. Forte, S. Marzani, and G. Ridolfi, *Top Quark Pair Production beyond NNLO*, *JHEP* **08** (2015) 076, [[arXiv:1505.02006](#)].

- [130] A. Broggio, A. Ferroglia, R. Frederix, D. Pagani, B. D. Pecjak, and I. Tsinikos, *Top-quark pair hadroproduction in association with a heavy boson at NLO+NNLL including EW corrections*, *JHEP* **08** (2019) 039, [[arXiv:1907.04343](#)].
- [131] **LHC Higgs Cross Section Working Group** Collaboration, D. de Florian et al., *Handbook of LHC Higgs Cross Sections: 4. Deciphering the Nature of the Higgs Sector*, [arXiv:1610.07922](#).
- [132] N. Kidonakis, *Theoretical results for electroweak-boson and single-top production*, *PoS DIS2015* (2015) 170, [[arXiv:1506.04072](#)].
- [133] S. Catani, L. Cieri, G. Ferrera, D. de Florian, and M. Grazzini, *Vector boson production at hadron colliders: a fully exclusive QCD calculation at NNLO*, *Phys. Rev. Lett.* **103** (2009) 082001, [[arXiv:0903.2120](#)].
- [134] G. Balossini, G. Montagna, C. M. Carloni Calame, M. Moretti, O. Nicrosini, F. Piccinini, M. Treccani, and A. Vicini, *Combination of electroweak and QCD corrections to single W production at the Fermilab Tevatron and the CERN LHC*, *JHEP* **01** (2010) 013, [[arXiv:0907.0276](#)].
- [135] B. Blok and F. A. Ceccopieri, *Z plus jets production via double parton scattering in pA collisions at the LHC*, *Eur. Phys. J. C* **80** (2020), no. 8 762, [[arXiv:2004.05186](#)].
- [136] C. Balazs, P. M. Nadolsky, C. Schmidt, and C. P. Yuan, *Diphoton background to Higgs boson production at the LHC with soft gluon effects*, *Phys. Lett. B* **489** (2000) 157–162, [[hep-ph/9905551](#)].
- [137] J. M. Campbell, J. Rojo, E. Slade, and C. Williams, *Direct photon production and PDF fits reloaded*, *Eur. Phys. J. C* **78** (2018), no. 6 470, [[arXiv:1802.03021](#)].
- [138] **ATLAS** Collaboration, G. Aad et al., *Observation of top-quark pair production in association with a photon and measurement of the  $t\bar{t}\gamma$  production cross section in pp collisions at  $\sqrt{s} = 7$  TeV using the ATLAS detector*, *Phys. Rev. D* **91** (2015), no. 7 072007, [[arXiv:1502.00586](#)].
- [139] X. Chen, T. Gehrmann, E. W. N. Glover, M. Höfer, A. Huss, and R. Schürmann, *Single photon production at hadron colliders at NNLO QCD with realistic photon isolation*, *JHEP* **08** (2022) 094, [[arXiv:2205.01516](#)].
- [140] H. A. Chawdhry, M. Czakon, A. Mitov, and R. Poncelet, *NNLO QCD corrections to diphoton production with an additional jet at the LHC*, *JHEP* **09** (2021) 093, [[arXiv:2105.06940](#)].
- [141] G. Bozzi, F. Campanario, V. Hankele, and D. Zeppenfeld, *NLO QCD corrections to  $W+W$ -gamma and  $Z Z$  gamma production with leptonic decays*, *Phys. Rev. D* **81** (2010) 094030, [[arXiv:0911.0438](#)].
- [142] Y.-B. Shen, R.-Y. Zhang, W.-G. Ma, X.-Z. Li, Y. Zhang, and L. Guo, *NLO QCD + NLO EW corrections to  $WZZ$  productions with leptonic decays at the LHC*, *JHEP* **10** (2015) 186, [[arXiv:1507.03693](#)]. [Erratum: *JHEP* 10, 156 (2016)].
- [143] S. D. Ellis, C. K. Vermilion, and J. R. Walsh, *Techniques for improved heavy particle searches with jet substructure*, *Phys. Rev. D* **80** (2009) 051501, [[arXiv:0903.5081](#)].
- [144] S. D. Ellis, C. K. Vermilion, and J. R. Walsh, *Recombination Algorithms and Jet Substructure: Pruning as a Tool for Heavy Particle Searches*, *Phys. Rev. D* **81** (2010) 094023, [[arXiv:0912.0033](#)].

- [145] J. Y. Araz, *Spey: Smooth inference for reinterpretation studies*, *SciPost Phys.* **16** (2024), no. 1 032, [[arXiv:2307.06996](#)].
- [146] A. Hocker et al., *TMVA - Toolkit for Multivariate Data Analysis*, [physics/0703039](#).
- [147] R. Brun, F. Rademakers, and S. Panacek, *ROOT, an object oriented data analysis framework*, in *CERN School of Computing (CSC 2000)*, pp. 11–42, 2000.
- [148] D. Krohn, M. D. Schwartz, T. Lin, and W. J. Waalewijn, *Jet Charge at the LHC*, *Phys. Rev. Lett.* **110** (2013), no. 21 212001, [[arXiv:1209.2421](#)].
- [149] J. Thaler and K. Van Tilburg, *Identifying boosted objects with  $n$ -subjettiness*, *Journal of High Energy Physics* **2011** (Mar., 2011).